Neurobiology of Disease 195 (2024) 106496

Contents lists available at ScienceDirect

Neurobiology of Disease

journal homepage: www.elsevier.com/locate/ynbdi

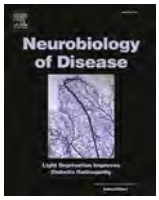

Phenotypic analysis of multielectrode array EEG biomarkers in developing and adult male *Fmr1* KO mice

Carrie R. Jonak [a], Samantha A. Assad [a], Terese A. Garcia [a], Manbir S. Sandhu [a], Jeffrey A. Rumschlag [b], Khaleel A. Razak [c,d], Devin K. Binder [a,c,*]

[a] Division of Biomedical Sciences, School of Medicine, University of California, Riverside, CA, United States of America
[b] Department of Otolaryngology-Head and Neck Surgery, Medical University of South Carolina, Charleston, SC, United States of America
[c] Neuroscience Graduate Program, University of California, Riverside, CA, United States of America
[d] Department of Psychology, University of California, Riverside, CA, United States of America

ARTICLE INFO

Keywords:
Fragile X syndrome
Autism spectrum disorders
Electroencephalography
Biomarker
Auditory cortex
Sensory hypersensitivity
EEG
Multielectrode array
Gamma power
Asymmetry

ABSTRACT

Fragile X Syndrome (FXS) is a leading known genetic cause of intellectual disability with symptoms that include increased anxiety and social and sensory processing deficits. Recent electroencephalographic (EEG) studies in humans with FXS have identified neural oscillation deficits that include increased resting state gamma power, increased amplitude of auditory evoked potentials, and reduced phase locking of sound-evoked gamma oscillations. Similar EEG phenotypes are present in mouse models of FXS, but very little is known about the development of such abnormal responses. In the current study, we employed a 30-channel mouse multielectrode array (MEA) system to record and analyze resting and stimulus-evoked EEG signals in male P21 and P91 WT and *Fmr1* KO mice. This led to several novel findings. First, P91, but not P21, *Fmr1* KO mice have significantly increased resting EEG power in the low- and high-gamma frequency bands. Second, both P21 and P91 *Fmr1* KO mice have markedly attenuated inter-trial phase coherence (ITPC) to spectrotemporally dynamic auditory stimuli as well as to 40 Hz and 80 Hz auditory steady-state response (ASSR) stimuli. This suggests abnormal temporal processing from early development that may lead to abnormal speech and language function in FXS. Third, we found hemispheric asymmetry of fast temporal processing in the mouse auditory cortex in WT but not *Fmr1* KO mice. Together, these findings define a set of EEG phenotypes in young and adult mice that can serve as translational targets for genetic and pharmacological manipulation in phenotypic rescue studies.

1. Introduction

Fragile X Syndrome (FXS) is the most common genetic cause of intellectual disability with symptoms that overlap with autism spectrum disorders (ASD) (Crawford et al., 2001). FXS is caused by a mutation in the *Fmr1* gene and a loss of Fragile X Messenger Ribonucleoprotein 1 (FMRP) (Yu et al., 1991). FMRP is an RNA-binding protein that regulates synaptic function through regulation of protein translation (Darnell et al., 2011). Symptoms associated with FXS include increased anxiety, repetitive behaviors, social communication deficits, delayed language development and abnormal sensory processing (Abbeduto and Hagerman, 1997; Berry-Kravis, 2002; Hagerman et al., 2009; Miller et al., 1999; Musumeci et al., 1999; Roberts et al., 2001; Sabaratnam et al., 2001; Sinclair et al., 2017b; Van der Molen et al., 2010; Wisniewski et al., 1991). Abnormal sensory processing in FXS includes hypersensitivity and reduced habituation to repeated sensory stimuli (Castrén et al., 2003; Schneider et al., 2013).

Auditory processing deficits are common in both humans with FXS (Castrén et al., 2003; Ethridge et al., 2016; Schneider et al., 2013; Van der Molen and Van der Molen, 2013) and *Fmr1* knockout (KO) mice (Lovelace et al., 2018; Lovelace et al., 2016; Razak et al., 2021; Rotschafer and Razak, 2013; Rotschafer and Razak, 2014; Wen et al., 2018), a mouse model of FXS (Bernardet and Crusio, 2006; Consorthium et al., 1994). EEG recordings from humans have shown altered cortical oscillatory activity that may contribute to sensory hypersensitivity and social communication deficits in FXS (Ethridge et al., 2017; Wang et al., 2017).

Abbreviations: ASD, autism spectrum disorder; ASSR, auditory steady-state response; EEG, electroencephalography; FMRP, Fragile X Messenger Ribonucleoprotein 1; FXS, Fragile X Syndrome; ITPC, inter-trial phase coherence; MEA, multielectrode array.

* Corresponding author at: Division of Biomedical Sciences, University of California, 900 University Avenue, Riverside, CA 92521, United States of America.
E-mail address: dbinder@ucr.edu (D.K. Binder).

https://doi.org/10.1016/j.nbd.2024.106496
Received 3 February 2024; Received in revised form 3 April 2024; Accepted 3 April 2024
Available online 4 April 2024

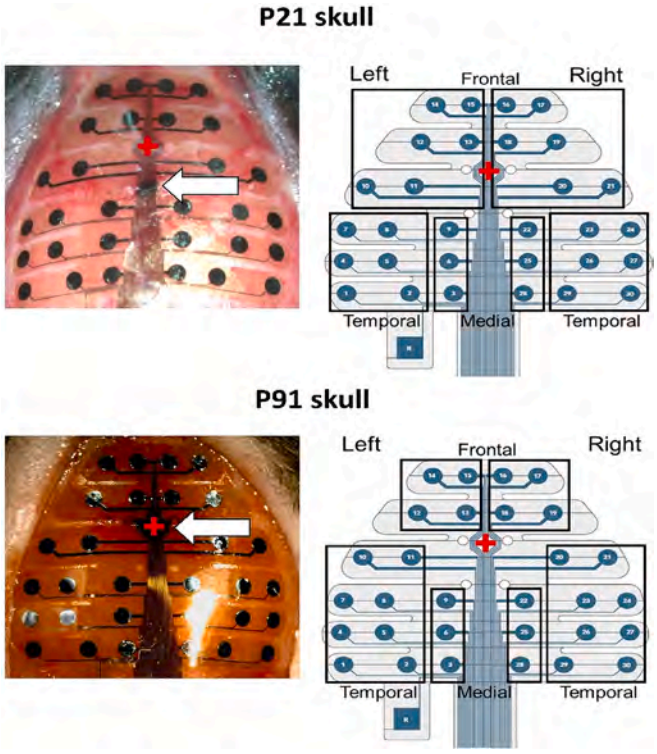

Fig. 1. Comparison of P21 *vs.* P91 MEA implantations. For P21 mice (*top*), the probe was placed on the skull surface carefully aligning the "+" in the center of the probe and advancing 1.0 mm anterior to bregma (*white arrow*). Due to the small size of the skull, this modification was necessary in order to position the probe over the exposed skull area. For P91 mice (*bottom*), the probe was placed on the skull surface carefully aligning the "+" in the center of the probe with bregma (*white arrow*) as we have previously done (Jonak et al., 2018; Jonak et al., 2020; Jonak et al., 2022; Jonak et al., 2021). Resulting electrode channel groupings are shown at right for P21 (*top*) and P91 (*bottom*) (frontal electrodes all anterior to bregma in each case).

Gamma band frequency power was enhanced in humans with FXS compared to healthy controls (Wang et al., 2017). When neural oscillations were induced with the spectrotemporally dynamic auditory "chirp" stimulus, inter-trial phase coherence (ITPC, phase-locking) was reduced in humans with FXS, particularly at gamma frequencies (Ethridge et al., 2017). This suggests abnormalities in temporal fidelity of responses across trials, a marker of impaired temporal processing that may underlie speech and language deficits in FXS (Shannon et al., 1995; Tallal et al., 1993). Indeed, these phenotypes were correlated with parent reports of social communication deficits and hypersensitive sensory responses suggesting clinical relevance of the EEG measures (Ethridge et al., 2019; Ethridge et al., 2017).

Identification of comparable biomarkers in humans and validated animal models is a critical step in facilitating pre-clinical to clinical therapeutic pipelines to treat neurodevelopmental disorders (Berry-Kravis et al., 2018). In particular, understanding the differences in biomarkers at different developmental ages is crucial for identification of treatment windows. To this end, we initially found enhanced resting state gamma power and reduced intertrial phase coherence (ITPC) to auditory "chirp" stimuli in adult *Fmr1* KO mice using epidural screw electrodes (Lovelace et al., 2018). Subsequently, we developed and applied multielectrode array (MEA) analysis in mice involving stable chronic *in vivo* implantation of a planar MEA on the surface of the mouse skull enabling low-noise 30-channel simultaneous EEG and resting and stimulus-evoked EEG acquisition in awake, freely moving mice (Jonak et al., 2018). This method allows examination of regional differences in EEG responses, and more closely aligns with human EEG work. Using the MEA system, we reported EEG phenotypes in adult *Fmr1* KO mice that are similar to those observed in humans including altered resting EEG power, event-related potentials (ERPs), single-trial and train-related EEG power, and ITPC to auditory chirp stimuli in *Fmr1* KO mice (Jonak et al., 2020).

In the current study, the major goal was to identify whether MEA EEG phenotypes are similar in developing (P21) mice and adult *Fmr1* KO (P91) mice. In particular, we tested whether both resting and sound-evoked EEG phenotypes were present early in development. To enable study of developmental phenotypes, we have adapted the *in vivo* MEA system to developing mice for the first time. Here, we report distinct MEA-derived EEG phenotypes in developing (P21) *vs.* adult *Fmr1* KO mice. Second, in addition to the auditory "chirp" stimulus, we have studied auditory steady-state response (ASSR). The ASSR has been used as a diagnostic biomarker for neurological disorders such as schizophrenia (Brenner et al., 2009; O'Donnell et al., 2013) and autism (Seymour et al., 2020), with potential age differences (Ono et al., 2020). Rather than interrogating a broad range of frequencies, the ASSR drives steady brain oscillations at specific frequencies of interest. Here, we report impaired ITPC to 40 and 80 Hz ASSR stimuli in P21 and adult *Fmr1* KO mice. Finally, we also report hemispheric asymmetry in fast temporal processing in the temporal cortex of WT but not *Fmr1* KO mice.

2. Methods

2.1. Animals

All procedures were approved by the Institutional Animal Care and Use Committee at the University of California, Riverside and in accordance with the NIH Animal Care and Use Guidelines. The mice used in this study were male wild-type (WT) and *Fmr1* KO mice on a C57BL/6 J background maintained in-house. The colony was established from breeding pairs of *Fmr1* KO (B6.129P2-Fmr1tm1Cgr/J, stock #003025) and C57BL/6 J WT (stock #000664) from Jackson Laboratory (Bar Harbor, ME). Hemizygous male and homozygous female *Fmr1* KO mice were bred to generate mutant mice. C57BL/6 WT male and WT female mice were bred to generate WT mice. The WT and KO mice were

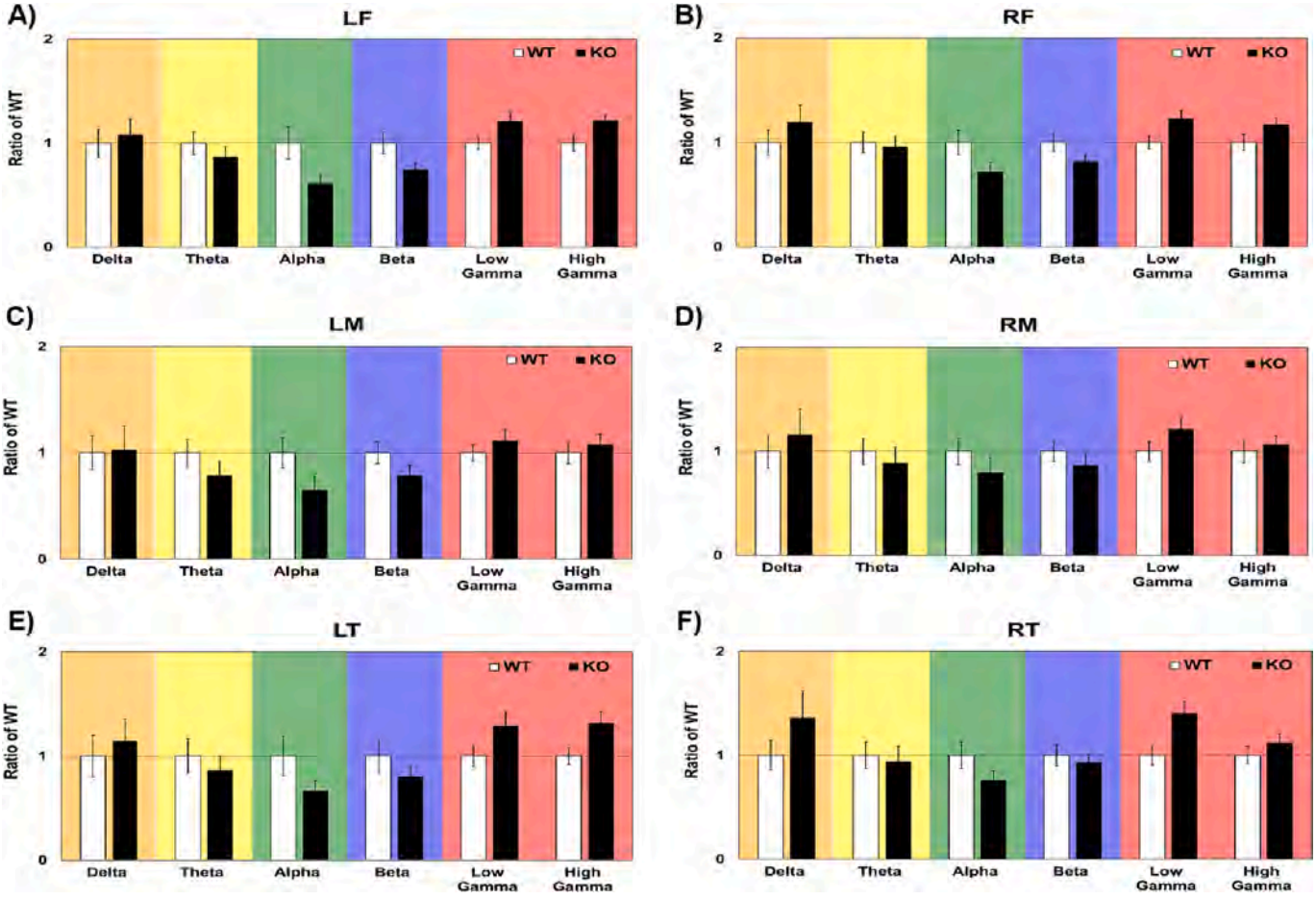

Fig. 2. Resting state power spectral density in P21 WT *vs. Fmr1* KO mice. Ratio of *Fmr1* KO (*black bars*) to WT (*white bars*) represent EEG resting state power across frequency bands for distinct brain regions (A–F). Values above 1 indicate higher EEG power in *Fmr1* KO compared with WT mice. Bars represent group means +/− standard error. LF, left frontal; RF, right frontal; LM, left medial; RM, right medial; LT, left temporal; RT, right temporal.

maintained in-house as individual strains. Mice generated were grouped-housed with two to five mice per cage. Mice were maintained in an AAALAC-accredited facility under a 12-h light/dark cycle and were provided irradiated rodent diet (PicoLab, 5053) and water *ad libitum*. All genotypes were confirmed by Transnetyx (Cordova, TN) using real-time PCR analysis. Developing mice (P20–21) and adult mice (P91–105) were used for this study, which we refer to as P21 and P91, respectively, with the following sample sizes: WT P21 ($n = 15$); P91 (n = 15), KO P21 (n = 15); P91 (n = 15).

2.2. Rationale for ages selected

We chose P21 in order to be congruent with previous papers demonstrating decreased PNN expression surrounding parvalbumin-positive interneurons and cortical hyperexcitability in *Fmr1* KO mice at P21 (Wen et al., 2018) and examination of developmental changes in EEG phenotypes in *Fmr1* KO mice (Wen et al., 2019). Additionally, the P14-P21 age corresponds to the critical period for responses to simple tones and maturation of tonotopic maps and inhibitory circuits in the auditory cortex (Carrasco et al., 2013; Kim et al., 2013; Oswald and Reyes, 2011) Finally, due to size limitations, it is not possible yet to implant the MEA in skulls younger than P18, and implantation surgery must be done 2–3 days prior to the recording. Therefore, using our technique we were able to implant at P18 and record at P21.

The adult (P91) age chosen was chosen to be consistent with our previous study to be able to compare data from different stimulus paradigms (Jonak et al., 2020). In addition, this is an age at which the mice are of fully reproductive age, but before the onset of functional accelerated hearing loss in the C57BL/6 J strain (Chawla and McCullagh, 2021; Spongr et al., 1997).

2.3. MEA implantation

Surgical and recording procedures were similar to those recently described (Jonak et al., 2020; Jonak et al., 2022; Jonak et al., 2021). Mice were anesthetized with isoflurane inhalation (0.2–0.5%) and given ketamine (80 mg/kg, i.p.) (Zoetis,10,004,027) and xylazine (10 mg/kg, i.p.) (Bimeda, 1XYL003). Mice were aseptically prepared for surgery and secured in a stereotaxic apparatus. Artificial tear ointment was applied to the eyes to prevent drying. Toe pinch reflex was used to measure anesthetic depth throughout the surgery, and supplemental doses of ketamine/xylazine were administered as needed. Once the mouse was anesthetized, a midline sagittal incision was made along the scalp to expose the skull. A cotton-tip applicator was used to remove the periosteum from the skull and to clean skull with saline. A surgical marker was used to mark bregma and positions of three screws. A dental drill was used to drill 1 mm diameter holes in the skull overlying the left frontal cortex, left cerebellum and right cerebellum. Screws (Protech International, 00–96 × 1/16) were advanced into drilled holes until secure; special care was taken not to advance the screws beyond the point of contact with the dura. Bregma was marked with a surgical marker and the probe grounding wire was placed in the nuchal musculature. Saline was added to the top of the skull to aid in probe adherence. For P21 mice, the probe (NeuroNexus, #EEG_v2-H32) was

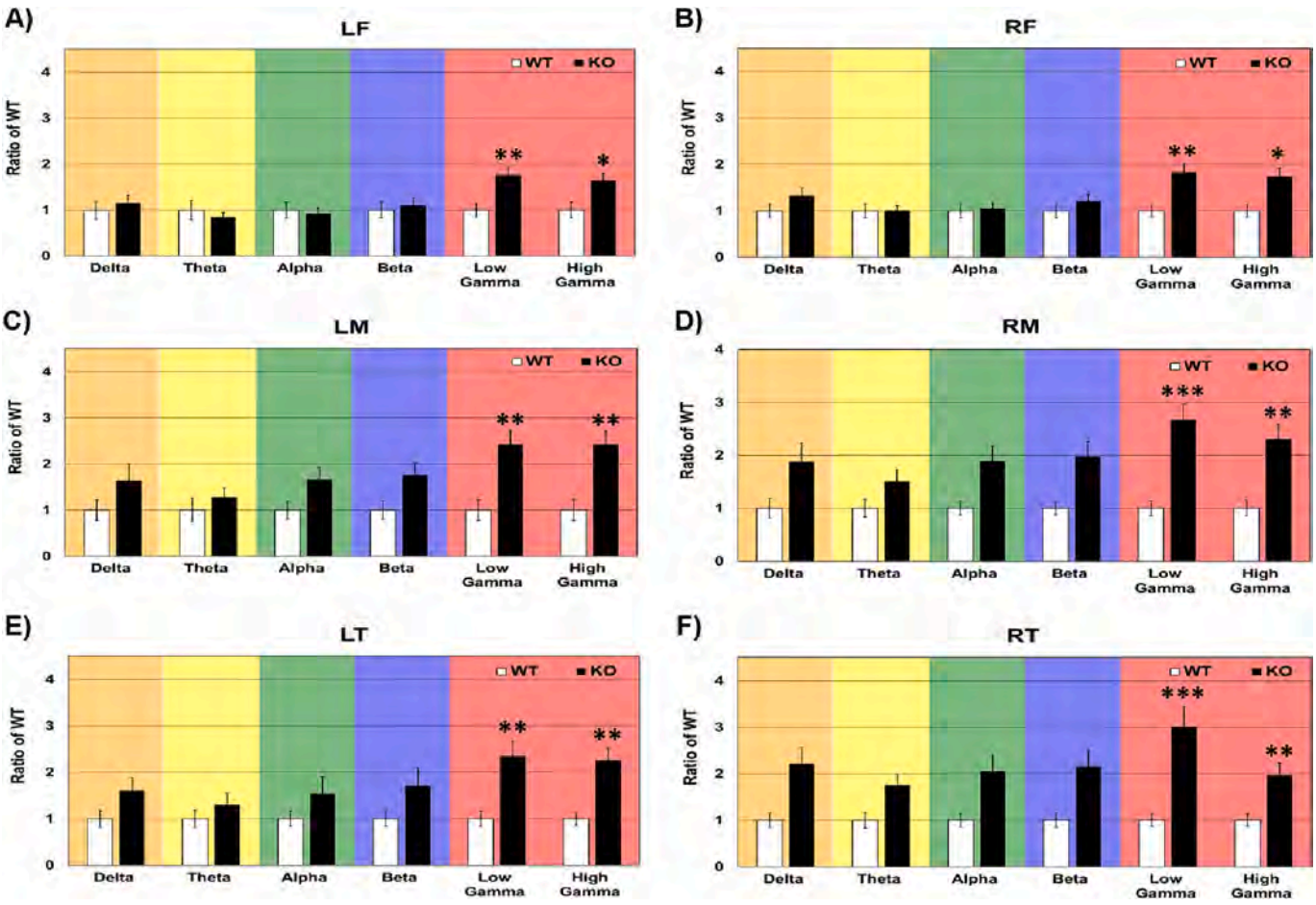

Fig. 3. Resting state power spectral density in P91 WT *vs. Fmr1* KO mice. Ratio of *Fmr1* KO (*black bars*) to WT (*white bars*) represent EEG resting state power across frequency bands for distinct brain regions (A–F). Values above 1 indicate higher EEG power in *Fmr1* KO compared with WT mice. Bars represent group means +/− standard error. Statistical significance (*$p < 0.05$; ** $p < 0.01$; *** $p < 0.001$). LF, left frontal; RF, right frontal; LM, left medial; RM, right medial; LT, left temporal; RT, right temporal.

placed on the skull surface carefully aligning the "+" in the center of the probe and advancing 1.0 mm anterior to bregma. Due to the small size of the skull, this modification was necessary in order to position the probe over the exposed skull area (Fig. 1). For P91 mice, the probe was placed on the skull surface carefully aligning the "+" in the center of the probe with bregma (Fig. 1). The saline was allowed to dry, and Teflon was placed on top of the probe. Dental cement (Kuraray, 3382KA) was applied around the screws, on the base of the cotton-tip applicator post, and the Teflon covering the probe. Waterproof medical tape was used to secure the cotton-tip applicator to the probe connector. Triple antibiotic was applied along the edges of the dental cement followed by a subcutaneous injection of 0.1 mg/kg buprenorphine (Reckitt & Colman, 5,053,624). Mice were placed on a heating pad to aid in recovery from anesthesia. P21 mice were group-housed (up to 5 mice) and P91 mice were individually housed. Additional doses of buprenorphine were administered every 6–8 h for continuous analgesia during the first 48 h after surgery. EEG recordings were conducted 2–3 days after MEA implantation.

2.4. EEG recording

All EEG recordings were conducted in a sound-attenuated chamber lined with anechoic foam (Gretch-Ken Industries, Oregon). EEG recordings were obtained from awake and freely moving mice using the SmartBox (NeuroNexus) acquisition system. The acquisition hardware was set to lower (0.5 Hz) and upper (500 Hz) filters and data were sampled at a rate of 1250 Hz. Mice were connected to a headstage, under brief isoflurane anesthesia, and tethered by a SmartLink cable to a freely rotating commutator positioned directly above a plastic arena. The plastic arena was surrounded by a Faraday cage securely fixed to a vibration isolation table. Mice were allowed to habituate to the arena for 20 min before EEG recordings were obtained.

2.5. Auditory stimulus presentation for EEG recordings

After mice were habituated, EEG was recorded for 5 min in the absence of any specific auditory stimulation ('resting state EEG'). Subsequently, acoustic stimulation was presented. To quantify the ability of neural generators to produce synchronized oscillations to time varying stimuli, we employed two types of auditory stimuli. The first type of stimulation is called the auditory chirp-modulated sound (henceforth, "chirp"). The chirp is a broadband noise stimulus whose amplitude is modulated using a sinusoid with increasing or decreasing frequency in the 1–100 Hz range (Artieda et al., 2004; Pérez-Alcázar et al., 2008; Purcell et al., 2004). The chirp facilitates a rapid measurement of evoked phase locking to auditory stimuli of varying frequencies and can be used to compare temporal processing in clinical and pre-clinical settings (Purcell et al., 2004). Inter-trial phase coherence (ITPC), also known as phase locking factor (Tallon-Baudry et al., 1996), can be used to determine the ability of neural generators to synchronize oscillations to the frequencies present across trials. Both humans with FXS and *Fmr1* KO mice show ITPC deficits in the gamma band frequencies (~40 Hz)

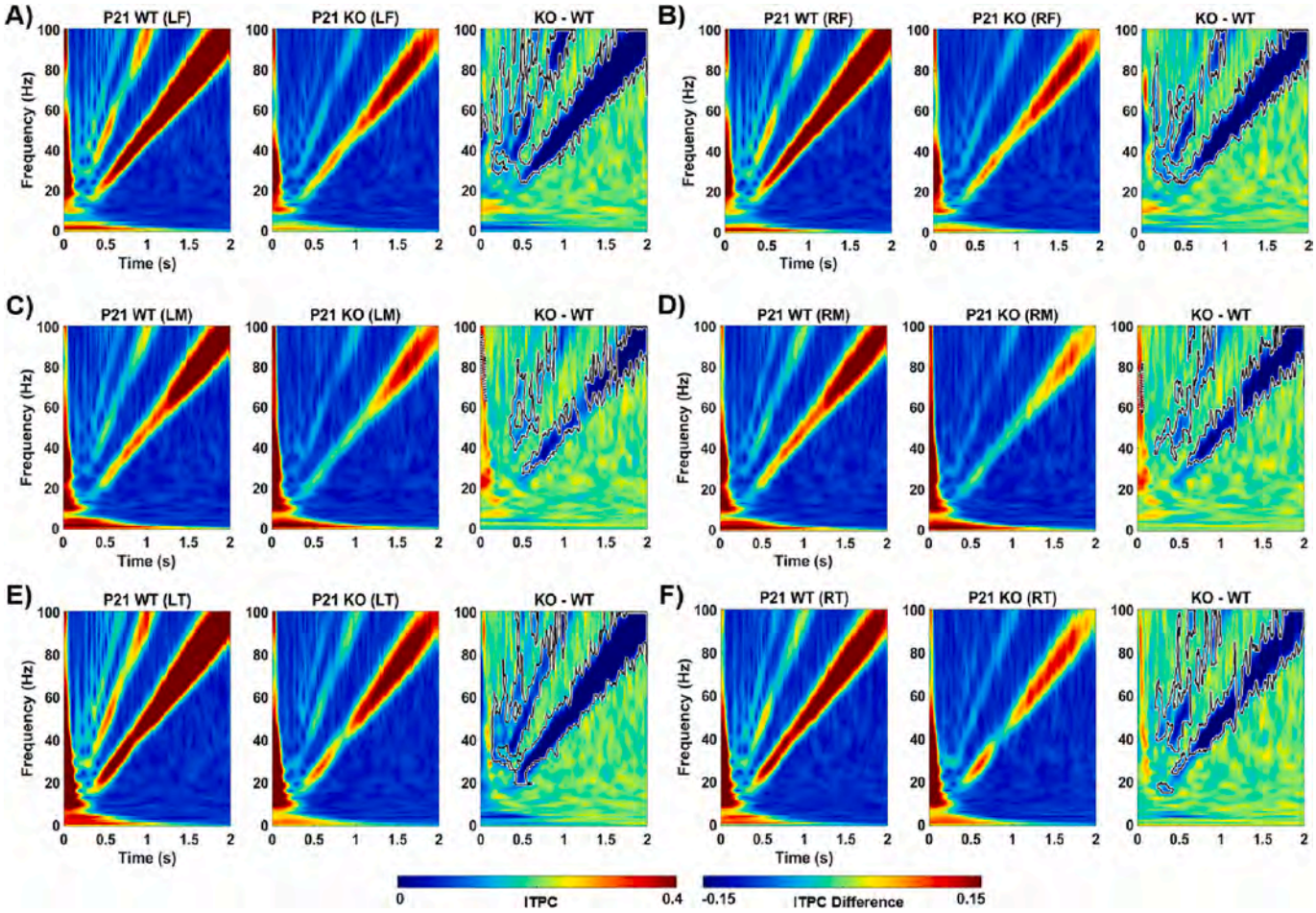

Fig. 4. Inter-trial phase coherence (ITPC) to auditory chirp stimulation in P21 WT *vs. Fmr1* KO mice. For each brain region (A-F), the left panel shows the averaged WT ITPC, the middle panel shows the averaged *Fmr1* KO ITPC, and the right panel shows KO-WT. Scales at the bottom show ITPC and ITPC difference in μV^2/Hz. Significant decreases in ITPC in *Fmr1* KO compared to WT mice are shown in black-outlined areas. Blue areas in the right panels (KO-WT) represent negative ITPC differences. LF, left frontal; RF, right frontal; LM, left medial; RM, right medial; LT, left temporal; RT, right temporal. (For interpretation of the references to colour in this figure legend, the reader is referred to the web version of this article.)

(Ethridge et al., 2017; Jonak et al., 2020; Jonak et al., 2022). In this study, each chirp stimulus was 2 s in duration, and the depth of modulation was 100%. Chirp trains were presented 200 times each with the interval between each train randomly generated to be between 1 and 1.5 s.

Second, we used a click train to assess the auditory steady-state response (ASSR). The ASSR has been used as a diagnostic biomarker for disorders such as schizophrenia (Brenner et al., 2009; O'Donnell et al., 2013). The ASSR drives steady brain oscillations at specific frequencies of interest. In this study, 40 and 80 Hz gamma frequencies were used to obtain ASSR, with the 40 Hz and 80 Hz generators likely located in cortex and brainstem, respectively (Pastor et al., 2002; Picton et al., 2003). The ASSR stimulus trains consisted of 0.5 ms clicks repeated at a rate of either 40 or 80 Hz over a 3 s period. Each train was presented 50 times with an inter-train interval of 2 s.

Acoustic stimuli were generated using RPVDSEX software and RZ6 hardware (Tucker Davis Technologies, FL) and presented through a free-field speaker (MF1 Multi-Field Magnetic Speaker; Tucker-Davis Technologies, FL) located 12 in. directly above the arena. Sound pressure level (SPL) was modified using programmable attenuators in the RZ6 system. The speaker output was ~70 dB SPL at the floor of the recording chamber with fluctuation of ±3 dB for frequencies between 5 and 35 kHz as measured with a ¼ inch Bruel & Kjaer microphone. Sound delivery was synchronized with EEG recordings using a TTL pulse to mark the onset of each sound in a train.

2.6. Statistical analyses

All EEG files extracted from SmartBox software were saved in a format compatible with Analyzer 2.2 (Brain Vision Inc). Resting EEG recordings were first down sampled to 625 Hz and notch filtered at 60 Hz to remove any residual line frequency power. A semi-automatic procedure implemented in Analyzer 2.2 was used for artifact rejection after visual inspection of all EEG files. <20% of data were rejected due to artifacts from any single animal recording.

Resting state data were divided into 1 s segments and each segment was subjected to Fast Fourier Transforms (FFT) analysis using a 10% Hanning window at 0.5 Hz bin resolution. The average power ($\mu V/Hz^2$) was calculated for each mouse from 1 to 100 Hz. Power was binned according to spectral frequency bands: Delta (1–4 Hz), Theta (4–8 Hz), Alpha (8–13 Hz), Beta (13–30 Hz), Low Gamma (30–55 Hz), and High Gamma (65–100 Hz).

Resting state EEG data were blinded and analyzed using two-way ANOVA with Genotype (WT, *Fmr1* KO) and Frequency (delta to gamma) for the cortical regions (left frontal, right frontal, left medial, right medial, left temporal and right temporal) as factors. Data were expressed as ratio of WT values to gauge relative differences in various factors using the same scale. Data were analyzed for each factor and corrected for using Bonferroni adjusted *p*-values. p values <0.05 were considered significant for ANOVA. In all cases where genotype means are reported, SEM was used. Statistical analyses were performed using

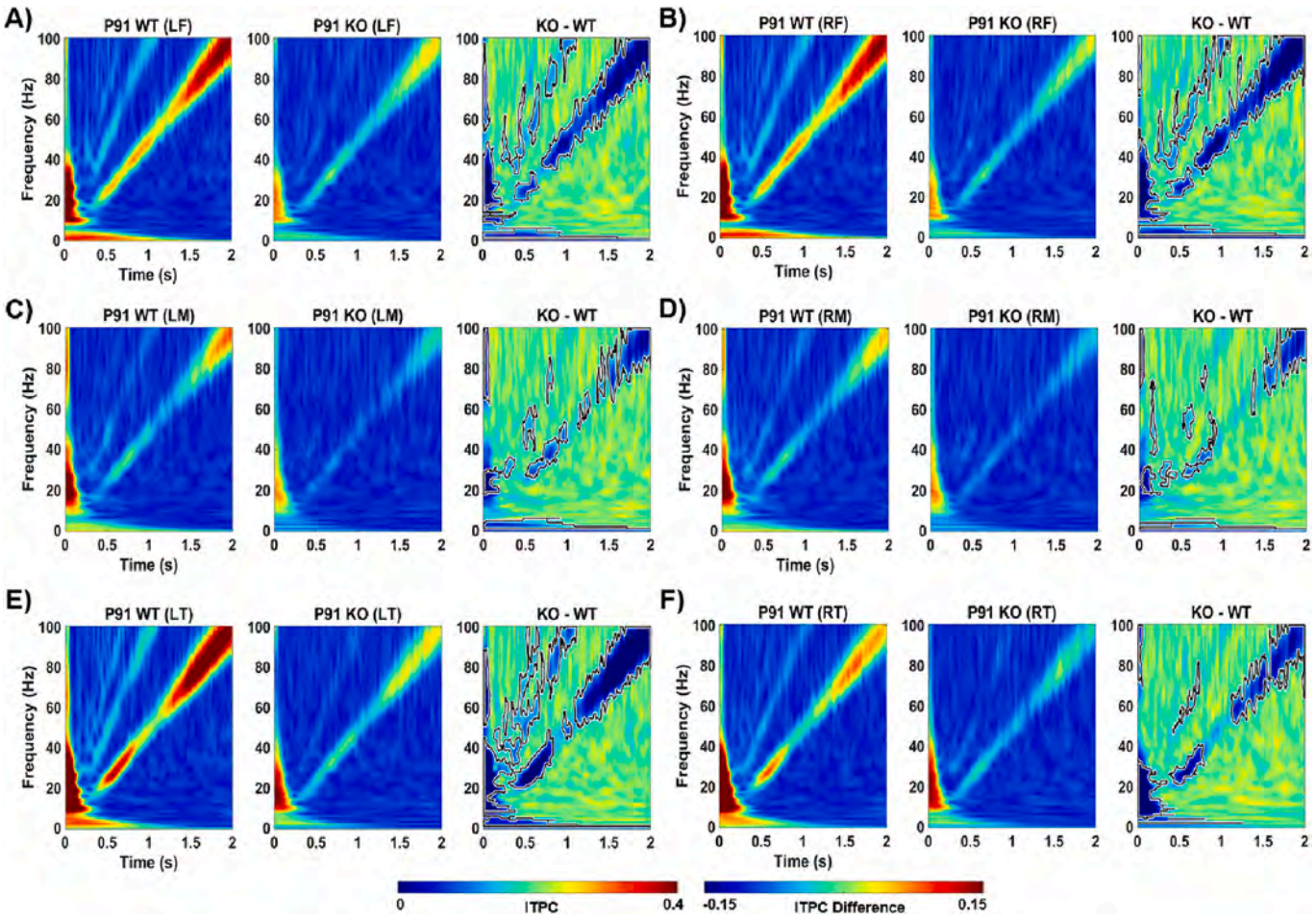

Fig. 5. Inter-trial phase coherence (ITPC) to auditory chirp stimulation in P91 WT *vs. Fmr1* KO mice. For each brain region (A-F), the left panel shows the averaged WT ITPC, the middle panel shows the averaged *Fmr1* KO ITPC, and the right panel shows KO-WT. Scales at the bottom show ITPC and ITPC difference in μV^2/Hz. Significant decreases in ITPC in *Fmr1* KO compared to WT mice are shown in black-outlined areas. Blue areas in the right panels (KO-WT) represent negative ITPC differences. LF, left frontal; RF, right frontal; LM, left medial; RM, right medial; LT, left temporal; RT, right temporal. (For interpretation of the references to colour in this figure legend, the reader is referred to the web version of this article.)

the program GraphPad Prism 9.5.1.

Chirp and ASSR traces were processed with Morlet wavelets linearly spaced from 1 to 100 Hz using voltage (μV). Wavelet coefficients were exported as complex values for use with inter-trial phase coherence (ITPC) analysis. Wavelets were run with a Morlet parameter of 10. To measure phase synchronization at each frequency across trials, ITPC was calculated as follows:

$$ITPC(f,t) = \frac{1}{n}\sum_{k=1}^{n}\frac{F_k(f,t)}{|F_k(f,t)|}$$

where *f* is the frequency, *t* is the time point, and *k* is trial number. Thus, $F_k(f,t)$ refers to the complex wavelet coefficient at a given frequency and time for the *k*th trial.

Statistical group comparisons of ITPC in chirp and ASSR (40 and 80 Hz) traces were quantified using a Monte Carlo permutation approach. Analysis was conducted by binning time into 256 parts and frequency into 100 parts, resulting in a 100 × 256 matrix. Non-parametric analysis was used to determine contiguous regions in the matrix that were significantly different from a distribution of 2000 randomized Monte Carlo permutations based on previously published methods (Maris and Oostenveld, 2007). Cluster sizes of the real genotype (both positive and negative direction, resulting in a two-tailed alpha of $p = 0.025$) that were larger than 97.25% of the random group assignments, were considered significantly different between genotypes. This method avoids statistical assumptions about the data and corrects for multiple comparisons.

3. Results

3.1. Resting state EEG power

Previously, we developed a method for stable chronic *in vivo* implantation of a planar MEA on the surface of the mouse skull (Jonak et al., 2018) featuring: (1) standardized implantation procedure; (2) reproducible placement of probe over the skull surface with bregma as reference; (3) Teflon/plastic wrap protective layer for the MEA probe to enable reusability; (4) secure implantation with dental cement and screw fixation; (5) fixation of the headstage with an anchoring "post"; (6) use of commutator to allow free movement of the mouse and cables without restriction; (7) reproducible artifact-free 30-channel EEG; and (8) reusability of the MEA probes. With this method, we reliably obtain 30-channel low-noise EEG from awake mice and previously used it to obtain resting and stimulus-evoked MEA EEG recordings in adult WT and *Fmr1* KO mice (Jonak et al., 2020).

Here, we applied the same MEA implantation technique to developing (P21) mice (Fig. 1). This required a 1 mm anterior modification of the placement position relative to bregma of the identical NeuroNexus planar MEA probe we use in adult (P91) mice. We found that secure implantation and fixation of the probe was feasible in the P21 mice,

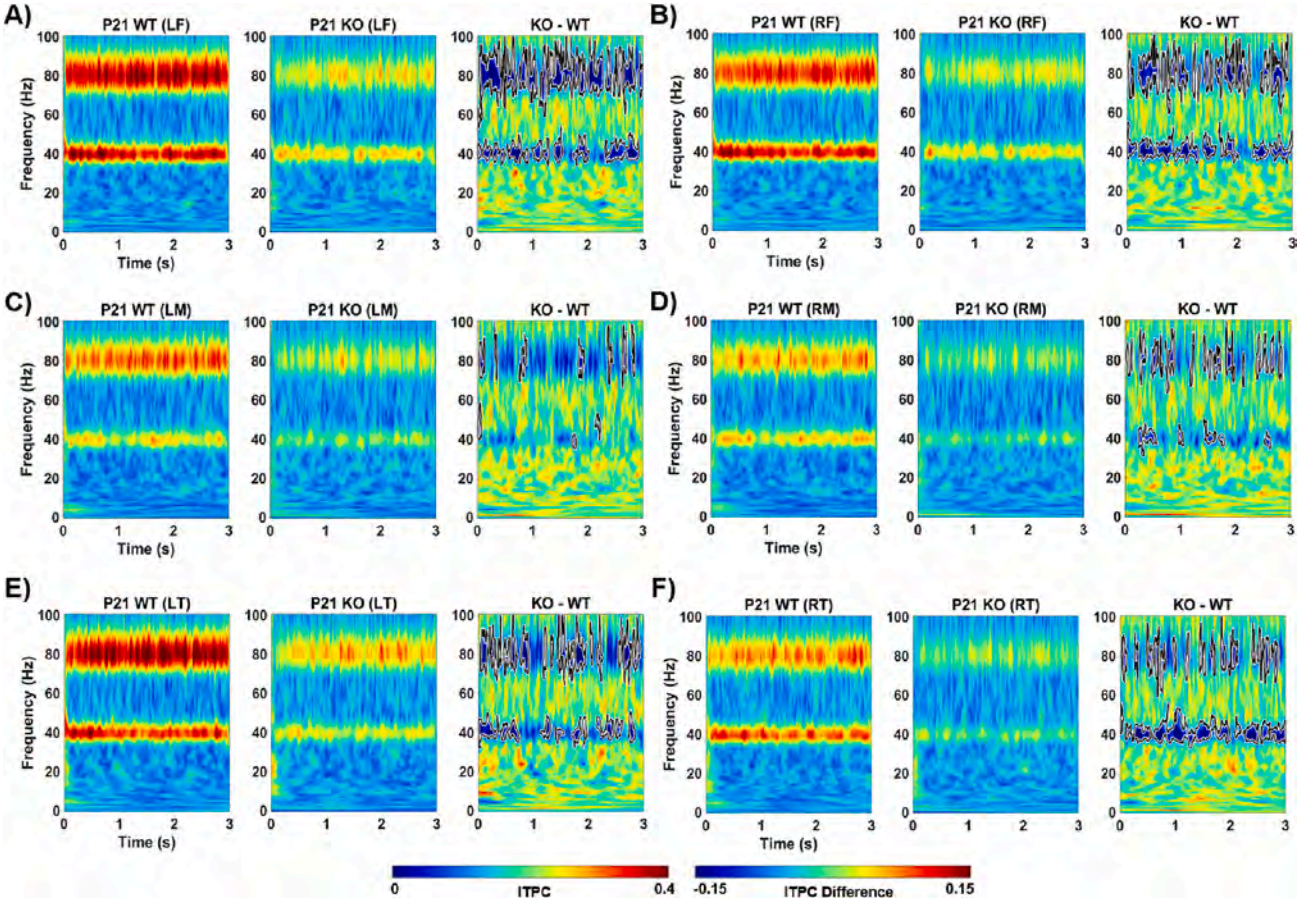

Fig. 6. Inter-trial phase coherence (ITPC) to 40 Hz auditory steady-state response (ASSR) in P21 WT *vs. Fmr1* KO mice. For each brain region (A-F), the left panel shows the averaged WT ITPC, the middle panel shows the averaged *Fmr1* KO ITPC, and the right panel shows KO-WT. Scales at the bottom show ITPC and ITPC difference in μV^2/Hz. Significant decreases in ITPC in *Fmr1* KO compared to WT mice are shown in black-outlined areas. Blue areas in the right panels (KO-WT) represent negative ITPC differences. LF, left frontal; RF, right frontal; LM, left medial; RM, right medial; LT, left temporal; RT, right temporal. (For interpretation of the references to colour in this figure legend, the reader is referred to the web version of this article.)

enabling recording of resting and stimulus-evoked EEG in freely-behaving P21 mice. Using the identical analysis that we use for adult mice, we found no difference in resting state power between P21 WT and P21 *Fmr1* KO mice ($n = 15$ each) **(**Fig. 2**).** In contrast, as we have previously found, we again found in a new cohort of P91 WT and *Fmr1* KO mice (n = 15 each) that adult *Fmr1* KO mice had significantly higher resting state low- and high-gamma power globally across brain areas **(**Fig. 3**).** These data confirm previous findings of increased gamma band EEG power in awake and freely moving adult *Fmr1* KO mice compared to WT mice (Jonak et al., 2020; Lovelace et al., 2018) and adduce the new observation that power spectral distributions are not different in P21 *Fmr1* KO *vs.* WT mice.

3.2. Auditory evoked responses

Inter-trial phase coherence (ITPC) measures the reliability of synchronization of neural responses to repetitions of auditory stimuli, with the EEG response entrained to the chirp modulation frequency or steady-state frequencies of interest. Markedly decreased chirp ITPC was seen globally across the brain in P21 and P91 *Fmr1* KO mice compared to WT age-matched mice **(**Figs. 4 and 5**)** (n = 15 each).

Next, we recorded 40 Hz ASSR with the MEA system in P21 and P91 WT and *Fmr1* KO mice (n = 15 each). In P21 WT mice, strong responses were observed, with a ITPC at 40 Hz and also a harmonic response at 80 Hz **(**Fig. 6**, left panels).** P21 *Fmr1* KO mice exhibited a markedly attenuated 40 Hz ASSR ITPC **(**Fig. 6**, middle panels).** Similarly, P91 WT mice exhibited a response to 40 Hz ASSR with 40 Hz ITPC and 80 Hz harmonic responses, although these were more region-specific than in P21 mice with weaker responses observed in "medial" regions **(**Fig. 7**, left panels, compare C and D to A, B, E, and F).** P91 *Fmr1* KO mice exhibited attenuated ITPC to 40 Hz ASSR compared with WT mice **(**Fig. 7**, middle panels).**

Next, we tested 80 Hz ASSR in P21 and P91 WT and *Fmr1* KO mice (n = 15 each). 40 and 80 Hz ASSR is thought to drive auditory cortex and auditory brainstem mediated responses, respectively (Pastor et al., 2002; Picton et al., 2003). In P21 WT mice, strong responses were observed to 80 Hz ASSR **(**Fig. 8**, left panels).** P21 *Fmr1* KO mice exhibited an attenuated 80 Hz ASSR ITPC **(**Fig. 8**, middle panels).** Similarly, to the case with 40 Hz ASSR, P91 WT mice exhibited a strong response to 80 Hz ASSR but this was region-specific with weaker responses observed in "medial" regions **(**Fig. 9**, left panels).** P91 *Fmr1* KO mice exhibited attenuated ITPC to 80 Hz ASSR compared with WT mice **(**Fig. 9**, middle panels).**

3.3. Hemispheric asymmetry

We observed a remarkable hemispheric asymmetry (left>right) in auditory evoked response synchronization, particularly in WT temporal cortex. To analyze this in further detail, we separated responses to auditory chirp, 40 Hz ASSR and 80 Hz ASSR by hemisphere and brain region and performed statistical comparisons using the identical Monte Carlo permutation approach (see Methods). For auditory chirp stimuli, we found left *vs.* right response asymmetries in WT mice in the temporal brain region (where auditory cortex resides) **(**Figs. 10 and 11**, left**

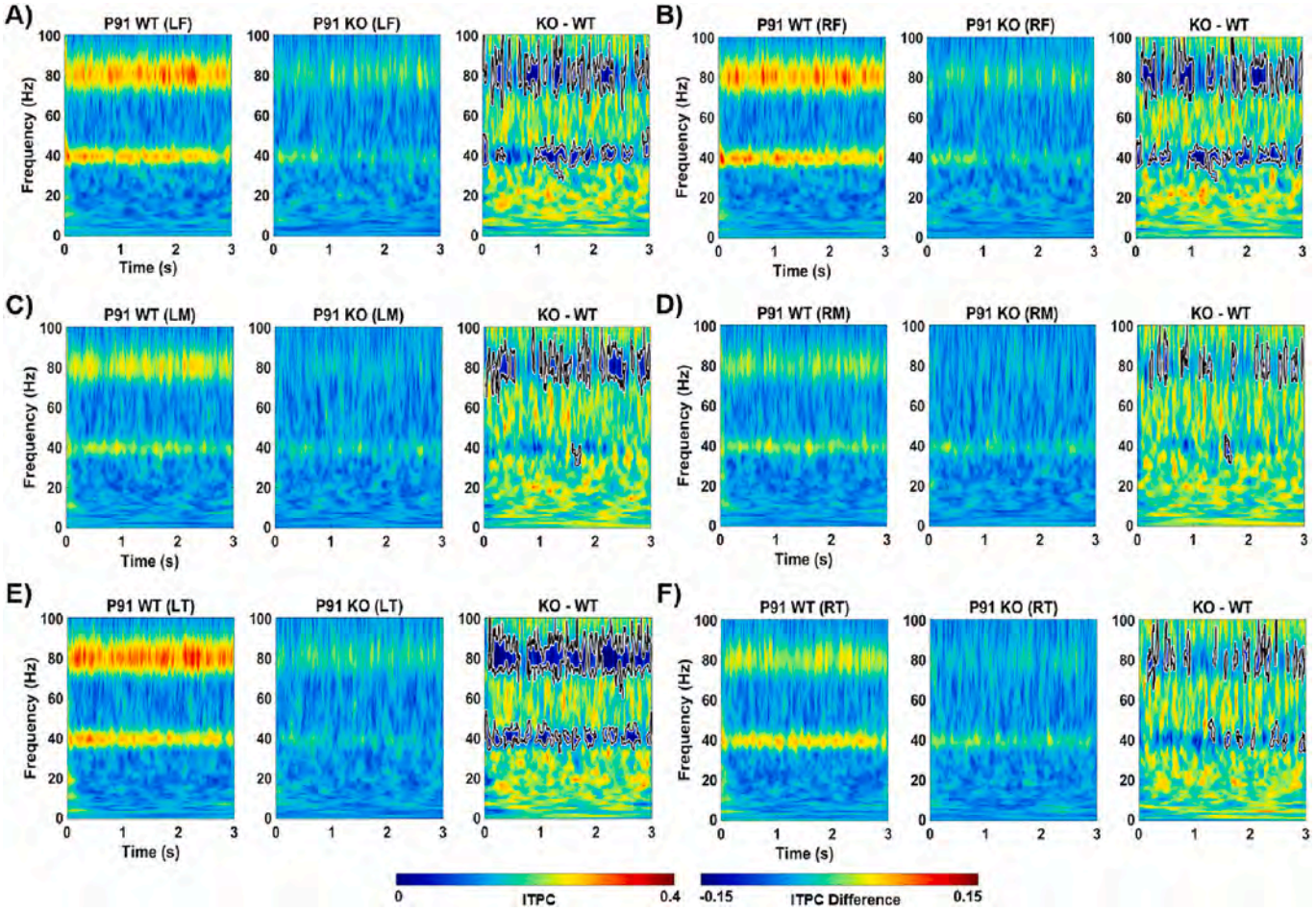

Fig. 7. Inter-trial phase coherence (ITPC) to 40 Hz auditory steady-state response (ASSR) in P91 WT *vs. Fmr1* KO mice. For each brain region (A-F), the left panel shows the averaged WT ITPC, the middle panel shows the averaged *Fmr1* KO ITPC, and the right panel shows KO-WT. Scales at the bottom show ITPC and ITPC difference in μV^2/Hz. Significant decreases in ITPC in *Fmr1* KO compared to WT mice are shown in black-outlined areas. Blue areas in the right panels (KO-WT) represent negative ITPC differences. LF, left frontal; RF, right frontal; LM, left medial; RM, right medial; LT, left temporal; RT, right temporal. (For interpretation of the references to colour in this figure legend, the reader is referred to the web version of this article.)

panels), but not for other electrode comparisons. Specifically, both P21 and P91 WT mice exhibited higher ITPC to auditory chirp stimuli in left compared to right temporal brain regions. However, this asymmetry was attenuated in P21 and P91 *Fmr1* KO mice (Figs. 10 and 11**, right panels).** Similarly, for 40 Hz (Figs. 12 and 13) and 80 Hz (Figs. 14 and 15) ASSR stimuli, we found left *vs.* right response asymmetries in WT mice in the temporal brain region, in particular in the 80 Hz response (Figs. 14 and 15**, left panels)**. Again, this asymmetry was attenuated in P21 and P91 *Fmr1* KO mice (Figs. 14 and 15**, right panels).**

4. Discussion

In this paper, we studied EEG biomarkers in P21 and adult *Fmr1* KO mice. This led to several novel findings. First, P91, but not P21, *Fmr1* KO mice have significantly increased resting state EEG power in the low- and high-gamma frequency bands. Second, both P21 and P91 *Fmr1* KO mice have markedly attenuated ITPC to auditory chirp stimuli as well as to 40 Hz and 80 Hz ASSR stimuli. Third, there is a remarkable hemispheric asymmetry (left>right) in auditory evoked response synchronization in the temporal cortex which is attenuated in *Fmr1* KO mice. Together, these findings define a set of EEG phenotypes that can serve as translational targets for genetic and pharmacological manipulation in phenotypic rescue studies at different ages.

4.1. Genotype and developmental differences in resting state EEG power spectral density

Increased resting state gamma (30–100 Hz) power is a well-described EEG phenotype in *Fmr1* KO mice (Jonak et al., 2020; Lovelace et al., 2018; Lovelace et al., 2020; Sinclair et al., 2017a; Wen et al., 2019), *Fmr1* KO rats (Berzhanskaya et al., 2017; Kozono et al., 2020), and in people with FXS (Ethridge et al., 2019; Ethridge et al., 2017; Wang et al., 2017). Our current findings using *in vivo* 30-channel MEA recordings confirm brain-wide increases in resting state low- and high-gamma power in adult (P91) *Fmr1* KO mice (Fig. 3). Interestingly, however, we did not observe any significant differences in resting EEG power in P21 *Fmr1* KO mice compared to age-matched WT mice (Fig. 2). This suggests that the gamma power phenotype observed across multiple studies in adult mice may develop subsequent to this developmental stage.

Gamma oscillations include both specific 40 Hz evoked rhythms and broadband gamma power, and the circuit mechanisms that generate power in these bands should be considered distinct (Ray and Maunsell, 2011). While in general there is strong support for the role of parvalbumin (PV) positive inhibitory interneurons in shaping 40 Hz evoked oscillatory rhythms (Buzsaki and Wang, 2012), the role of these neurons in the generation of broadband gamma oscillations appears reversed. The elevated broadband gamma (low and high) power in adult *Fmr1* KO mice may reflect reduced inhibition arising from PV interneurons. Loss

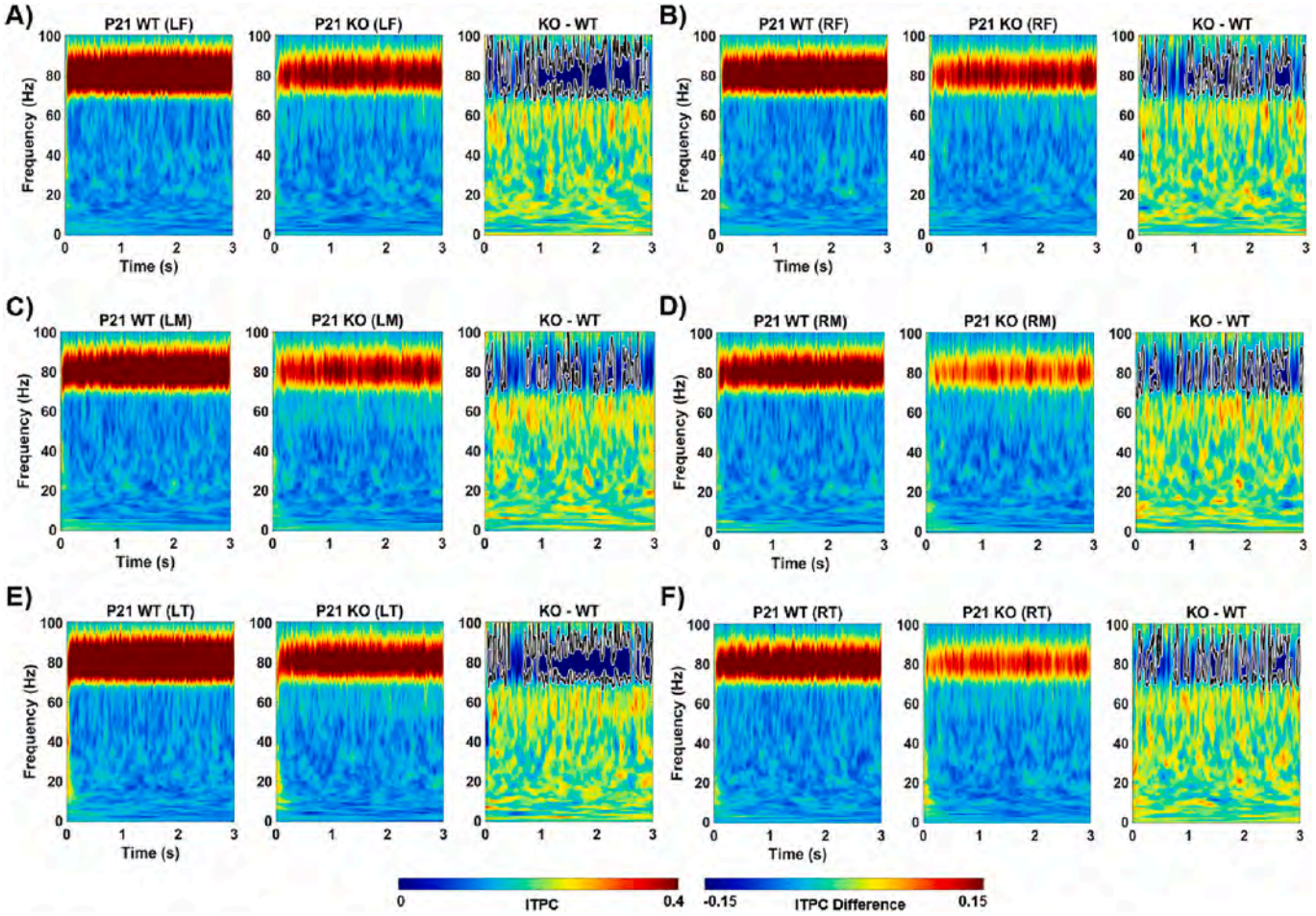

Fig. 8. Inter-trial phase coherence (ITPC) to 80 Hz auditory steady-state response (ASSR) in P21 WT *vs. Fmr1* KO mice. For each brain region (A-F), the left panel shows the averaged WT ITPC, the middle panel shows the averaged *Fmr1* KO ITPC, and the right panel shows KO-WT. Scales at the bottom show ITPC and ITPC difference in μV^2/Hz. Significant decreases in ITPC in *Fmr1* KO compared to WT mice are shown in black-outlined areas. Blue areas in the right panels (KO-WT) represent negative ITPC differences. LF, left frontal; RF, right frontal; LM, left medial; RM, right medial; LT, left temporal; RT, right temporal. (For interpretation of the references to colour in this figure legend, the reader is referred to the web version of this article.)

of NMDA receptor driven excitation of PV neurons (PV neuron hypofunction model) elevates broadband gamma power (Billingslea et al., 2014; Korotkova et al., 2010). Billingslea et al. also showed that baclofen administration in the PV hypofunction mice reduced resting state gamma power (Billingslea et al., 2014), a finding similar to data showing reduced resting state gamma power in *Fmr1* KO mice and humans with FXS after baclofen administration (Jonak et al., 2022). Carlén et al. showed similarly elevated broadband gamma power in PV neuron hypofunction model mice (Carlén et al., 2012). In these mice, optogenetically evoked gamma rhythms were reduced, suggesting different mechanisms for evoked and baseline gamma rhythms. This finding relates to our suggestion that PV neuron dysfunction leads to increased gamma band resting state power, while at the same time reduces ITPC to evoked gamma oscillations in *Fmr1* KO mice. Guyon et al. showed that long term deficits in PV neuron function are related to increased and asynchronous firing in the cortical network, manifesting as increased gamma power in local field potentials (Guyon et al., 2021). Indeed, recordings in both adult and P21 *Fmr1* KO mice show increased firing rates in the auditory cortex (Rotschafer and Razak, 2013; Wen et al., 2018). At least in the young mice, the elevated firing is due to abnormal development of PV neurons, and the perineuronal nets (PNN) that surround PV neurons (Wen et al., 2018). Normalization of PNNs around PV neurons reduced sound driven firing rates in auditory cortex of *Fmr1* KO mice (Wen et al., 2018). These findings, together with data reported here, suggest that long term PV neuron dysfunction in cortical networks of adult *Fmr1* KO mice gives rise to elevated broadband gamma power, but not yet at P21. A previous study reported increased resting state gamma power in both frontal and auditory cortex of *Fmr1* KO mice at P30 (Wen et al., 2019), suggesting the P21–30 developmental window as one where broadband gamma power increases, and maybe a potential target window for intervention. Future studies will be able to test whether pharmacological or genetic manipulation at this stage of development may be able to rescue the increased resting state gamma phenotype observed in adult mice (Razak et al., 2020).

4.2. Genotype and developmental differences in chirp synchronization

In addition to alterations in gamma power, recent EEG studies of humans with FXS reduced chirp-evoked phase locking in gamma frequencies (Ethridge et al., 2019; Ethridge et al., 2017; Wang et al., 2017). These EEG abnormalities were correlated with clinically relevant measures including heightened sensory sensitivity and autism-associated social impairment (Social Communication Questionnaire), indicating translational relevance (Ethridge et al., 2019; Ethridge et al., 2017). Given the recent human data indicating reduced chirp-evoked phase locking in gamma frequencies, we previously tested whether this could be reliably observed in the *Fmr1* KO mice with MEA analysis. Indeed, we observed a marked impairment in ITPC or "phase-locking" to chirp stimuli in adult *Fmr1* KO mice (Jonak et al., 2020) indicating abnormal spectrotemporal processing in adult *Fmr1* KO mice. In the current study,

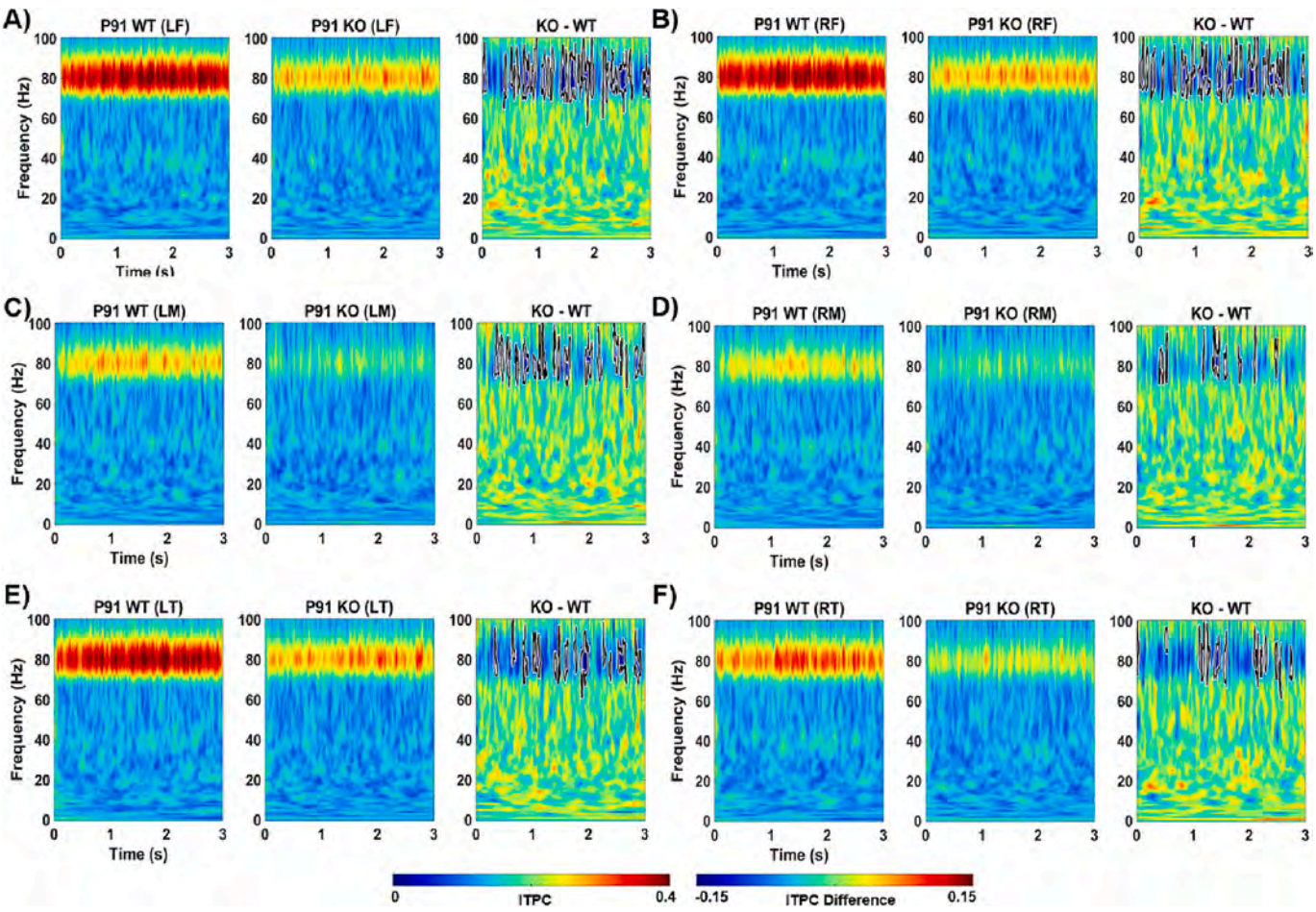

Fig. 9. Inter-trial phase coherence (ITPC) to 80 Hz auditory steady-state response (ASSR) in P91 WT *vs. Fmr1* KO mice. For each brain region (A-F), the left panel shows the averaged WT ITPC, the middle panel shows the averaged *Fmr1* KO ITPC, and the right panel shows KO-WT. Scales at the bottom show ITPC and ITPC difference in μV^2/Hz. Significant decreases in ITPC in *Fmr1* KO compared to WT mice are shown in black-outlined areas. Blue areas in the right panels (KO-WT) represent negative ITPC differences. LF, left frontal; RF, right frontal; LM, left medial; RM, right medial; LT, left temporal; RT, right temporal. (For interpretation of the references to colour in this figure legend, the reader is referred to the web version of this article.)

we replicated the chirp phenotype in adult *Fmr1* KO mice (Fig. 5) in a new cohort of mice, providing evidence for the consistency of these phenotypes. In addition, we show novel data that significant chirp ITPC deficits are seen as early as P21 in the *Fmr1* KO mice across all brain skull electrode locations (Fig. 4). Thus, auditory chirp stimulation may be a reliable EEG biomarker to distinguish stimulus-induced brain responses in P21 WT *vs. Fmr1* KO mice. Given the dissociation between lack of a resting state gamma power phenotype and the presence of a chirp phenotype in the P21 mice, it would be of great interest to study resting state gamma *vs.* chirp at the appropriate stage in children with FXS (Dutta and Sengupta, 2016; Ethridge et al., 2019; Ethridge et al., 2017; Pressler and Auvin, 2013; Semple et al., 2013; Swanson et al., 2018).

4.3. Genotype and developmental differences in auditory steady-state response

The auditory steady-state response (ASSR) is a stimulus rate-dependent, evoked response to constant periodic auditory stimuli that can be detected using EEG. ASSRs show a peak response at 40 Hz across species, and may mark a cortical resonance frequency for acoustic input (Picton et al., 2003). 40 Hz ASSRs were originally used to show reduced power and phase delay to 40-Hz stimulation in subjects with schizophrenia (Kwon et al., 1999), which provided support for the hypothesis of compromised gamma band oscillations in schizophrenia (Uhlhaas and Singer, 2010). Subsequent studies have converged on using 40 Hz ASSR as a diagnostic biomarker for schizophrenia (Brenner et al., 2009; Grent-'t-Jong et al., 2023; O'Donnell et al., 2013). Unlike transient evoked potentials, ASSRs require high temporal resolution for coordinated signal integration; thus, the ASSR response not only reflects early event-related potential processes but also the generation of sustained rhythmic activity at the frequency of interest (Grent-'t-Jong et al., 2023). This is of potentially significant interest in FXS as well given the known abnormalities in gamma band resting state power and induced synchrony to broadband chirp stimuli.

Here, we report markedly impaired ITPC to 40 (Figs. 6–7) and 80 Hz (Figs. 8–9) ASSR stimuli in P21 and adult *Fmr1* KO mice across all electrodes, suggesting a brain wide impairment in generating steady-state gamma oscillations. The genotypic differences appear equally as consistent as the differences in chirp ITPC (Figs. 4–5). Of note, a recent study also found reduced responses to 40 Hz ASSR in *Fmr1* KO rats, and the authors concluded that 40 Hz ASSR may be a cross-species translational biomarker (Kozono et al., 2020). It is thought that 40 Hz oscillations emerge from the synchronization of pyramidal cell firing by PV interneurons (Buzsaki and Wang, 2012; Cardin et al., 2009; Wang

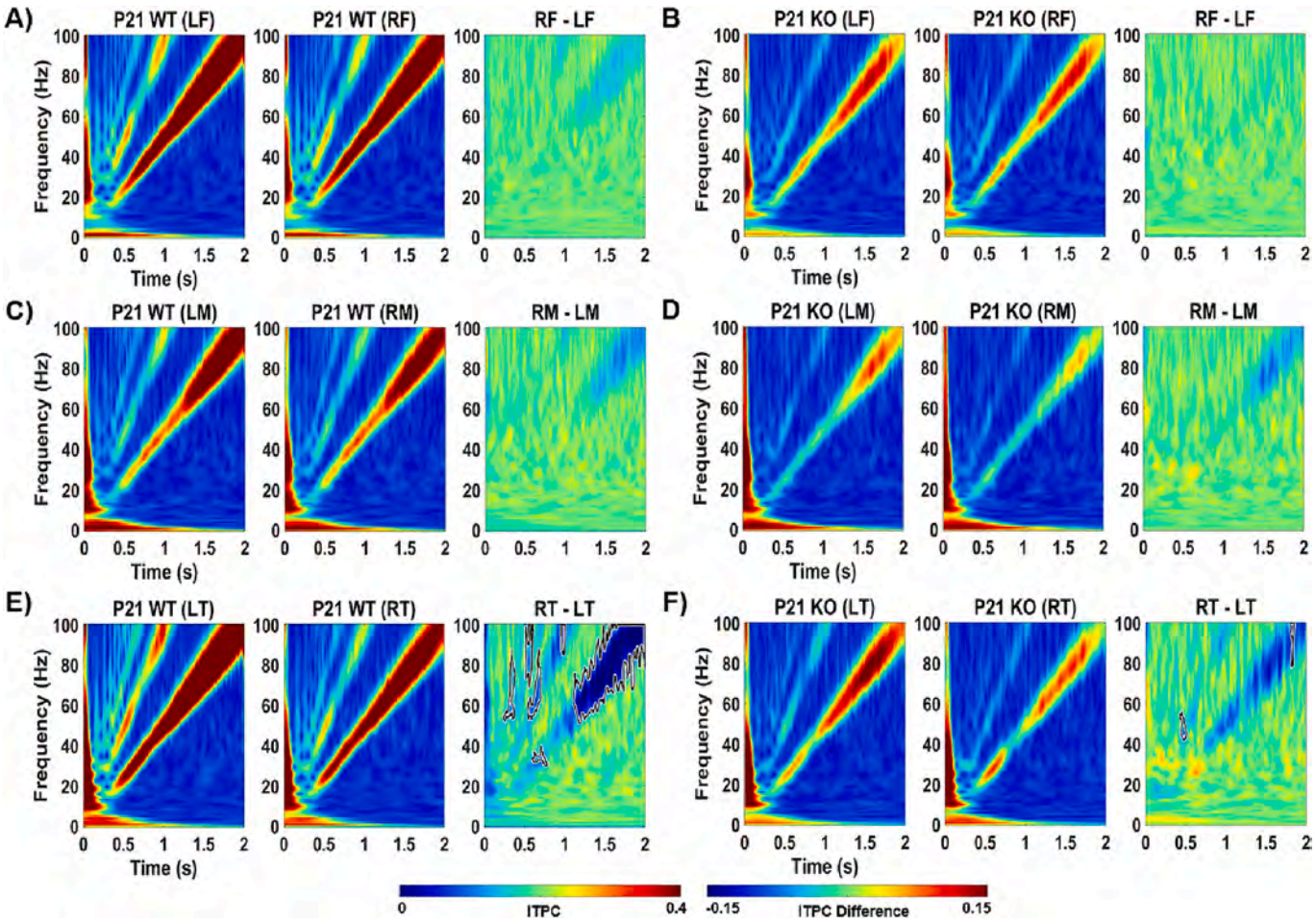

Fig. 10. P21 hemispheric asymmetry in response to auditory chirp stimulation. For each brain region, the left panel shows the averaged left hemisphere ITPC, the middle panel shows the averaged right hemisphere ITPC, and the right panel shows the difference (right-left). Scales at the bottom show ITPC and ITPC difference in μV^2/Hz.Significant decreases in ITPC in right *vs.* left are shown in black-outlined areas. Blue areas in the right panels represent negative ITPC differences. LF, left frontal; RF, right frontal; LM, left medial; RM, right medial; LT, left temporal; RT, right temporal. (For interpretation of the references to colour in this figure legend, the reader is referred to the web version of this article.)

and Buzsaki, 1996; Whittington et al., 1995). Pharmacological (Vohs et al., 2010) and optogenetic (Hwang et al., 2019) evidence also indicates that GABAergic neurotransmission modulates 40 Hz ASSRs (Grent-'t-Jong et al., 2023). It has also been suggested that NMDA receptor activation on PV cells is necessary for 40 Hz ASSR (Nakao et al., 2020; Sivarao, 2015). Thus, deficits in PV-related inhibition in FXS (Gibson et al., 2008; Goel et al., 2018; Wen et al., 2018), particularly through reduced NMDA receptor function, could potentially be responsible for abnormal ASSR observed in the *Fmr1* KO mice (this study) and *Fmr1* KO rats (Kozono et al., 2020). Further studies with genetic and/or pharmacological manipulation in *Fmr1* KO mice will be of interest to delineate the circuit mechanisms for abnormally attenuated ASSR responses in *Fmr1* KO mice, and the effects of normalizing ASSR parameters on perceptual/cognitive processing. In addition, the precise role of cortical *vs.* subcortical networks in the generation of the 40 *vs.* 80 Hz ASSR responses remains to be determined (Pastor et al., 2002; Picton et al., 2003). Overall, these ASSR findings together with the wealth of chirp ITPC data suggest a response "timing" deficit across the brain in *Fmr1* KO mice, *Fmr1* KO rats, and humans with FXS. Consistent with this notion, a recent study found significant deficits in the ability of cortical generators of *Fmr1* KO mice to register brief gaps in noise during early development (Croom et al., 2023). Thus, the available evidence indicates that ASSRs may be a promising biomarker for FXS processing deficits, even during early development. ASSR paradigms are currently being tested in children with FXS in parallel with chirp stimuli, which should help to determine the translational validity of these ASSR findings, and to test our prediction based on the current mouse data that the chirp/ASSR response synchronization deficits develop earlier than the gamma power abnormality in humans with FXS.

4.4. Hemispheric asymmetry

An interesting observation in WT mice using the MEA recording system is the presence of asymmetry of fast temporal processing in the mouse auditory cortex. Notably, the left *versus* right response asymmetries were present only in WT and *Fmr1* KO mice (WT > KO), and were predominantly seen only for high frequencies (high gamma band in chirp and 80 Hz ASSR) and when comparing the temporal electrodes. In human speech processing, considerable evidence exists for left hemispheric specialization for speech components with fast temporal modulations, while the right hemisphere may be specialized for slower modulations and spectral information (Giraud and Poeppel, 2012;

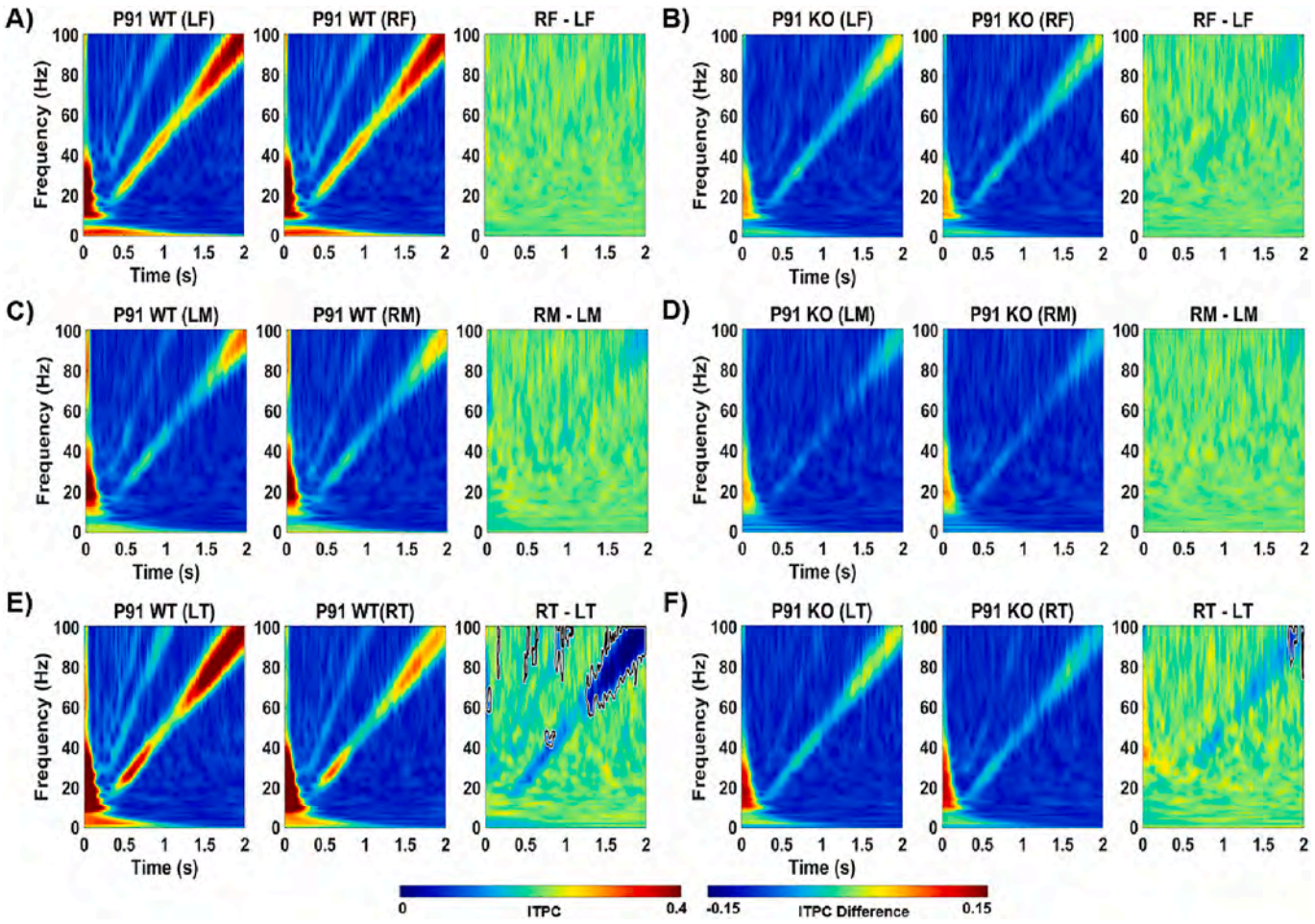

Fig. 11. P91 hemispheric asymmetry in response to auditory chirp stimulation. For each brain region, the left panel shows the averaged left hemisphere ITPC, the middle panel shows the averaged right hemisphere ITPC, and the right panel shows the difference (right-left). Scales at the bottom show ITPC and ITPC difference in μV^2/Hz.Significant decreases in ITPC in right *vs.* left are shown in black-outlined areas. Blue areas in the right panels represent negative ITPC differences. LF, left frontal; RF, right frontal; LM, left medial; RM, right medial; LT, left temporal; RT, right temporal. (For interpretation of the references to colour in this figure legend, the reader is referred to the web version of this article.)

Zatorre, 2022). Fast and slow temporal processing correspond to short and long temporal integration windows that allow for bilateral, but asymmetric, processing of speech. This 'asymmetric sampling of speech' theory purports that the left hemisphere is specialized for processing phonetic cues, while the right hemisphere may facilitate representation of intonation-type cues. The mouse MEA data is also supportive of better temporal processing (higher ITPC) for the chirp and 80 Hz ASSR stimuli in the left hemisphere compared to the right. Such asymmetry is strongest in the temporal regions where the auditory cortices reside. Our data are consistent with other studies of auditory cortex that reveal functional asymmetries in WT mice (Calhoun et al., 2023; Levy et al., 2019) and other species including gerbils (Wetzel et al., 2008), rats (Rybalko et al., 2010), mustached bats (Washington and Kanwal, 2012) and non-human primates (Petersen et al., 1978). Underlying circuit asymmetries for lateralization in auditory processing in mice have been suggested including hemispheric differences in inputs to specific inhibitory neurons (Oviedo, 2017) and differences in recurrent excitatory connections and connectivity between cortical layers (Levy et al., 2019). Synaptic connectivity patterns are affected by the loss of FMRP (Zhang et al., 2021), and may underlie the observed absence of asymmetries in ASSR or chirp ITPC in the *Fmr1* KO mice. Alternatively, the ITPC in *Fmr1* KO mice may simply be very low in both hemispheres (a floor effect) leading to the lack of asymmetries. In the ASD literature, studies have suggested abnormal lateralization patterns (Escalante-Mead et al., 2003; Stroganova et al., 2007). Abnormal lateralization may lead to language impairments in ASD (Lindell and Hudry, 2013). Given that temporal processing is critical for speech and language function (Shannon et al., 1995), our MEA observations in the present study using temporal processing may form a useful bridge to understand the structural and circuit basis of speech impairments in ASD. Future studies should investigate asymmetries in short- and long-range connectivity patterns in *Fmr1* KO mice that underlie differences in lateralization of temporal processing. We observe that hemispheric asymmetry in ITPC is present at both P21 and P91 in WT mice. It is unclear whether the development of asymmetry requires auditory experience because considerable experience-dependent plasticity occurs between hearing onset (~P11) in mice and P21, including the maturation of fast-spiking parvalbumin positive interneurons (Wen et al., 2018) and inhibitory circuitry (Oswald and Reyes, 2011). Future studies should be designed to examine potential asymmetry in chirp and ASSR synchronization in P12–14 mice.

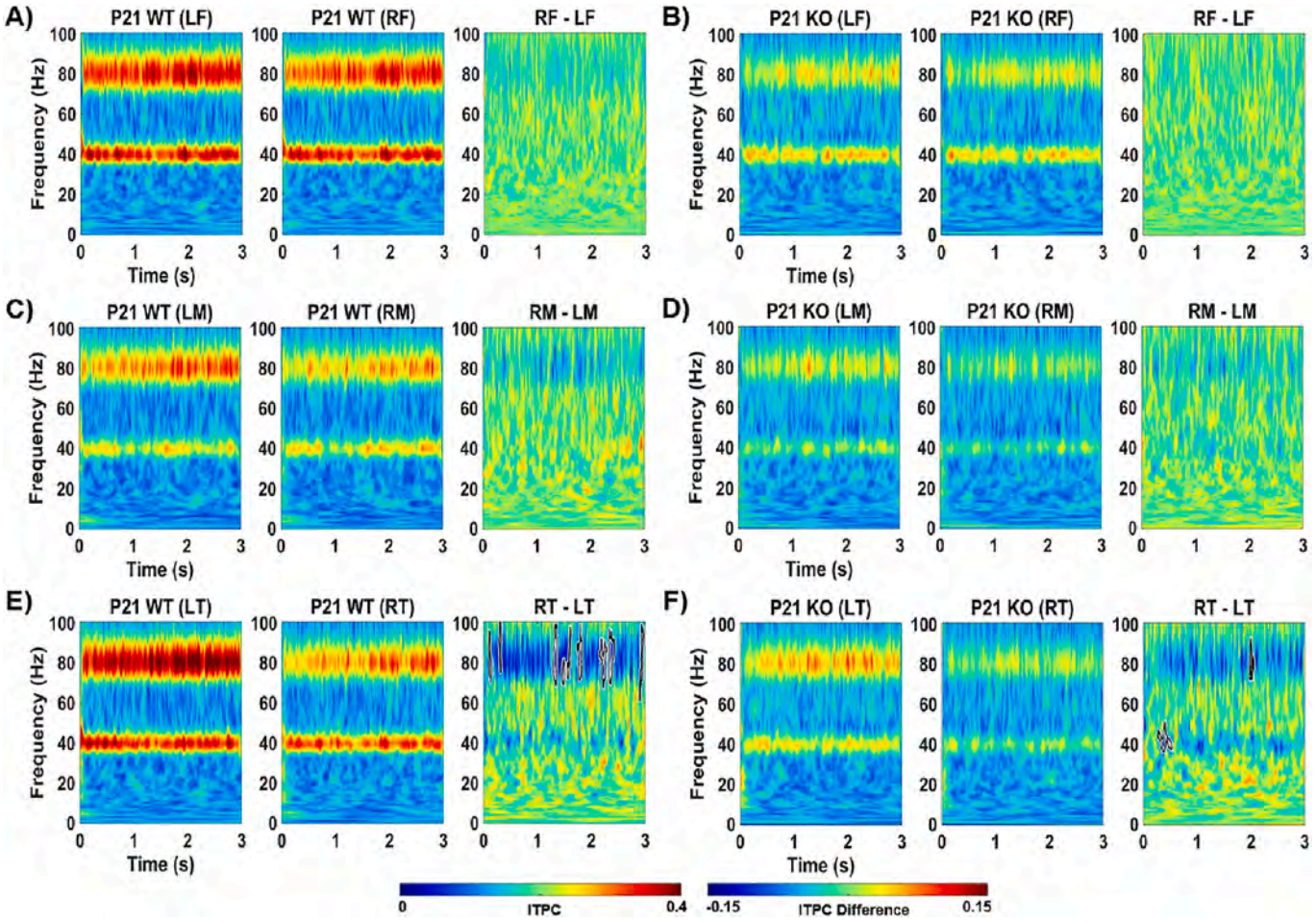

Fig. 12. P21 hemispheric asymmetry in response to 40 Hz auditory steady-state response. For each brain region, the left panel shows the averaged left hemisphere ITPC, the middle panel shows the averaged right hemisphere ITPC, and the right panel shows the difference (right-left). Scales at the bottom show ITPC and ITPC difference in μV^2/Hz. Significant decreases in ITPC in right *vs.* left are shown in black-outlined areas. Blue areas in the right panels represent negative ITPC differences. LF, left frontal; RF, right frontal; LM, left medial; RM, right medial; LT, left temporal; RT, right temporal. (For interpretation of the references to colour in this figure legend, the reader is referred to the web version of this article.)

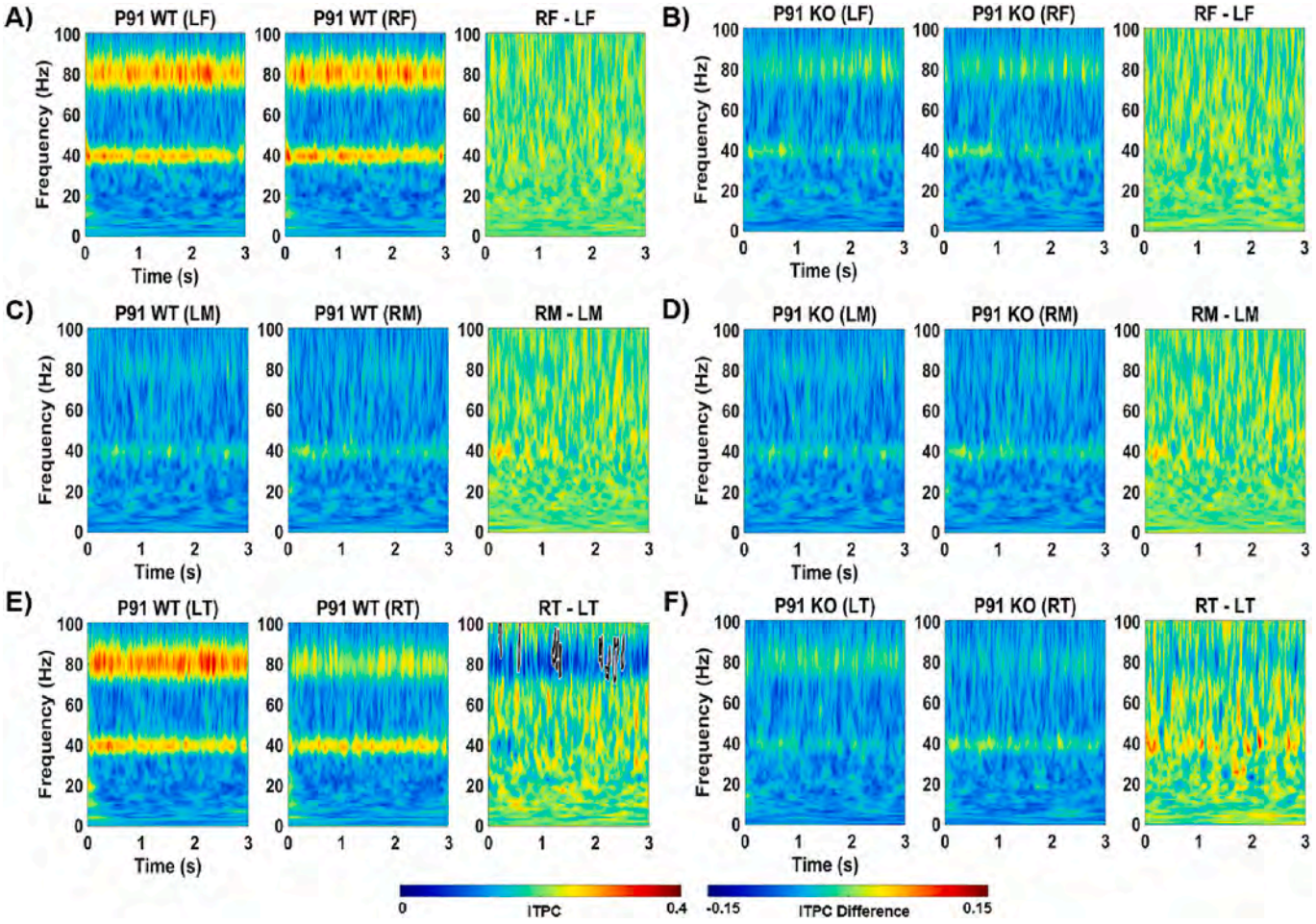

Fig. 13. P91 hemispheric asymmetry in response to 40 Hz auditory steady-state response. For each brain region, the left panel shows the averaged left hemisphere ITPC, the middle panel shows the averaged right hemisphere ITPC, and the right panel shows the difference (right-left). Scales at the bottom show ITPC and ITPC difference in μV^2/Hz. Significant decreases in ITPC in right *vs.* left are shown in black-outlined areas. Blue areas in the right panels represent negative ITPC differences. LF, left frontal; RF, right frontal; LM, left medial; RM, right medial; LT, left temporal; RT, right temporal. (For interpretation of the references to colour in this figure legend, the reader is referred to the web version of this article.)

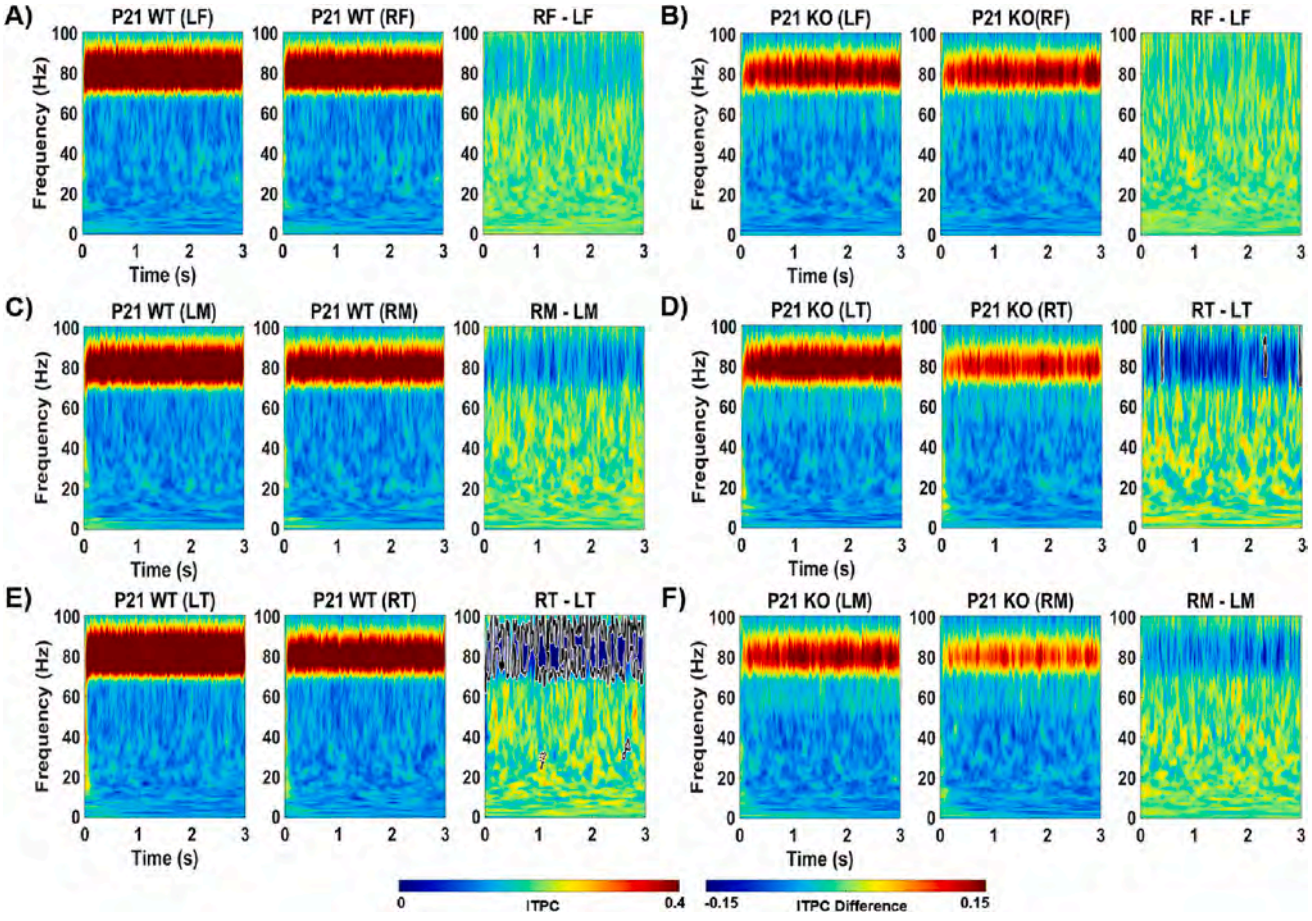

Fig. 14. P21 hemispheric asymmetry in response to 80 Hz auditory steady-state response. For each brain region, the left panel shows the averaged left hemisphere ITPC, the middle panel shows the averaged right hemisphere ITPC, and the right panel shows the difference (right-left). Scales at the bottom show ITPC and ITPC difference in μV^2/Hz. Significant decreases in ITPC in right *vs.* left are shown in black-outlined areas. Blue areas in the right panels represent negative ITPC differences. LF, left frontal; RF, right frontal; LM, left medial; RM, right medial; LT, left temporal; RT, right temporal. (For interpretation of the references to colour in this figure legend, the reader is referred to the web version of this article.)

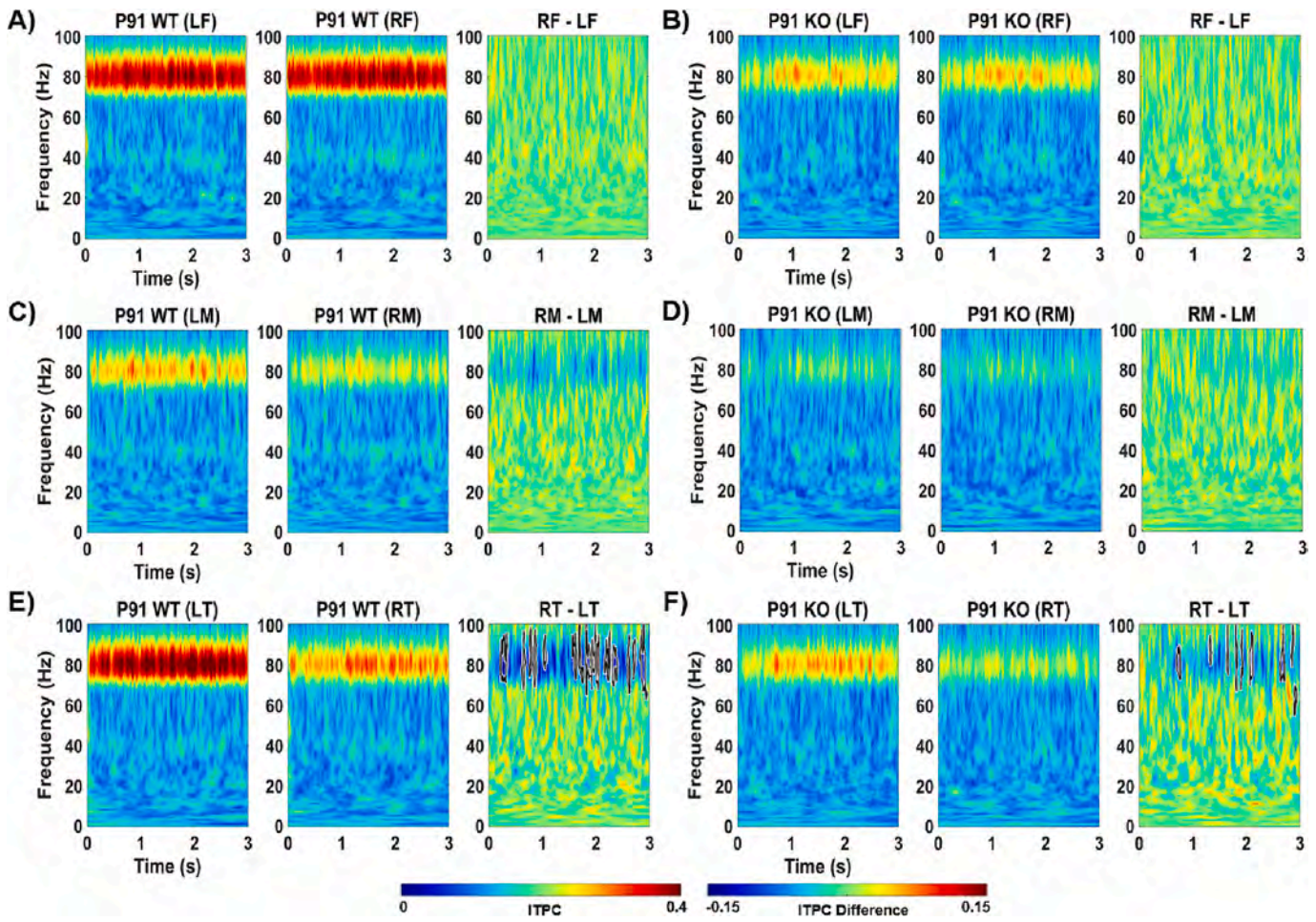

Fig. 15. P91 hemispheric asymmetry in response to 80 Hz auditory steady-state response. For each brain region, the left panel shows the averaged left hemisphere ITPC, the middle panel shows the averaged right hemisphere ITPC, and the right panel shows the difference (right-left). Scales at the bottom show ITPC and ITPC difference in μV^2/Hz. Significant decreases in ITPC in right *vs.* left are shown in black-outlined areas. Blue areas in the right panels represent negative ITPC differences. LF, left frontal; RF, right frontal; LM, left medial; RM, right medial; LT, left temporal; RT, right temporal. (For interpretation of the references to colour in this figure legend, the reader is referred to the web version of this article.)

4.5. Using mouse multielectrode array electroencephalography as a translational strategy

Similarity in EEG measures between humans and mice indicates that EEG recordings can serve as objective, physiological probes that serve as surrogate biomarkers to develop therapeutics to treat symptoms of FXS (Berry-Kravis et al., 2018; Ewen et al., 2019; Kenny et al., 2022; Schneider et al., 2013; Sinclair et al., 2017a). These measures may be useful outcome measures in the preclinical to clinical drug development pipeline and can be also employed in stratification of patient population for appropriate treatment strategies using a combination of EEGs and pharmacology (Berry-Kravis et al., 2018; Lee et al., 2018). In particular, the finding that a particular drug candidate (or genetic manipulation) normalizes EEG parameters such as resting state gamma power and phase-locked synchronization in both humans and mice would enable targeting and correlation of those drugs (or genetic manipulations) with clinical parameters (Berry-Kravis et al., 2018). Integration of human and animal model work in the context of developmental circuit mechanisms is of critical importance to identify age-specific outcome measures in treatment development (Razak et al., 2020). Examining multiple EEG responses (resting state power, evoked transient and steady state responses, hemispheric asymmetry) provides a range of outcomes, and underlying circuit mechanisms, to examine mechanisms of pathophysiology in FXS, as well as identify appropriate responses for clinical testing. Thus, the MEA system can serve as a useful method for further definition of EEG biomarkers in diverse disorders as well as an enabling technology for mechanistic and therapeutic studies.

CRediT authorship contribution statement

Carrie R. Jonak: Writing – review & editing, Validation, Methodology, Formal analysis, Data curation, Conceptualization. **Samantha A. Assad:** Methodology, Investigation, Formal analysis, Data curation. **Manbir S. Sandhu:** Methodology, Investigation. **Terese A. Garcia:** Methodology, Investigation, Data curation. **Jeffrey A. Rumschlag:** Methodology, Investigation, Formal analysis. **Khaleel A. Razak:** Writing – review & editing, Supervision, Funding acquisition, Formal analysis, Conceptualization. **Devin K. Binder:** Writing – review & editing, Writing – original draft, Validation, Supervision, Resources, Project administration, Methodology, Investigation, Funding acquisition, Formal analysis, Data curation, Conceptualization.

Declaration of competing interest

We report no conflicts of interest.

Data availability

Data will be made available on request.

Acknowledgements

We thank Lauren Ethridge, Ernie Pedapati, Craig Erickson, John Sweeney, Kim Huber, Jay Gibson, and Mike Ragozzino for intellectual collaboration and discussions. We dedicate this paper to the memory of our dear colleague John Sweeney. This work was supported by the National Institutes of Health (NIH) (1U54HD104461–01).

References

Abbeduto, L., Hagerman, R.J., 1997. Language and communication in fragile X syndrome. Ment. Retard. Dev. Disabil. Res. Rev. 3, 313–322.
Artieda, J., et al., 2004. Potentials evoked by chirp-modulated tones: a new technique to evaluate oscillatory activity in the auditory pathway. Clin. Neurophysiol. 115, 699–709.
Bernardet, M., Crusio, W.E., 2006. Fmr1 KO mice as a possible model of autistic features. Sci. World J. 6, 1164–1176.
Berry-Kravis, E., 2002. Epilepsy in fragile X syndrome. Dev. Med. Child Neurol. 44, 724–728.
Berry-Kravis, E.M., et al., 2018. Drug development for neurodevelopmental disorders: lessons learned from fragile X syndrome. Nat. Rev. Drug Discov. 17, 280–299.
Berzhanskaya, J., et al., 2017. Disrupted cortical state regulation in a rat model of fragile X syndrome. Cereb. Cortex 27, 1386–1400.
Billingslea, E.N., et al., 2014. Parvalbumin cell ablation of NMDA-R1 causes increased resting network excitability with associated social and self-care deficits. Neuropsychopharmacology 39, 1603–1613.
Brenner, C.A., et al., 2009. Steady state responses: electrophysiological assessment of sensory function in schizophrenia. Schizophr. Bull. 35, 1065–1077.
Buzsaki, G., Wang, X.J., 2012. Mechanisms of gamma oscillations. Annu. Rev. Neurosci. 35, 203–225.
Calhoun, G., et al., 2023. Bilateral widefield calcium imaging reveals circuit asymmetries and lateralized functional activation of the mouse auditory cortex. Proc. Natl. Acad. Sci. USA 120, e2219340120.
Cardin, J.A., et al., 2009. Driving fast-spiking cells induces gamma rhythm and controls sensory responses. Nature 459, 663–667.
Carlén, M., et al., 2012. A critical role for NMDA receptors in parvalbumin interneurons for gamma rhythm induction and behavior. Mol. Psychiatry 17, 537–548.
Carrasco, M.M., et al., 2013. Development of response selectivity in the mouse auditory cortex. Hear. Res. 296, 107–120.
Castrén, M., et al., 2003. Augmentation of auditory N1 in children with fragile X syndrome. Brain Topogr. 15, 165–171.
Chawla, A., McCullagh, E.A., 2021. Auditory brain stem responses in the C57BL/6J fragile X syndrome-knockout mouse model. Front. Integr. Neurosci. 15, 803483.
Consorthium, T. D.-B. F. X, et al., 1994. Fmr1 knockout mice: a model to study fragile X mental retardation. The Dutch-Belgian Fragile X Consortium. Cell 78, 23–33.
Crawford, D.C., et al., 2001. FMR1 and the fragile X syndrome: human genome epidemiology review. Genet. Med. 3, 359–371.
Croom, K., et al., 2023. Developmental delays in cortical auditory temporal processing in a mouse model of fragile X syndrome. J. Neurodev. Disord. 15, 23.
Darnell, Jennifer C., et al., 2011. FMRP stalls ribosomal translocation on mRNAs linked to synaptic function and autism. Cell 146, 247–261.
Dutta, S., Sengupta, P., 2016. Men and mice: relating their ages. Life Sci. 152, 244–248.
Escalante-Mead, P.R., et al., 2003. Abnormal brain lateralization in high-functioning autism. J. Autism Dev. Disord. 33, 539–543.
Ethridge, L.E., et al., 2016. Reduced habituation of auditory evoked potentials indicate cortical hyperexcitability in fragile X syndrome. Transl. Psychiatry 6, e787.
Ethridge, L.E., et al., 2017. Neural synchronization deficits linked to cortical hyperexcitability and auditory hypersensitivity in fragile X syndrome. Mol. Autism. 8, 22.
Ethridge, L.E., et al., 2019. Auditory EEG biomarkers in fragile X syndrome: clinical relevance. Front. Integr. Neurosci. 13, 60.
Ewen, J.B., et al., 2019. Conceptual, regulatory and strategic imperatives in the early days of EEG-based biomarker validation for neurodevelopmental disabilities. Front. Integr. Neurosci. 13, 45.
Gibson, J.R., et al., 2008. Imbalance of neocortical excitation and inhibition and altered UP states reflect network hyperexcitability in the mouse model of fragile X syndrome. J. Neurophysiol. 100, 2615–2626.
Giraud, A.L., Poeppel, D., 2012. Cortical oscillations and speech processing: emerging computational principles and operations. Nat. Neurosci. 15, 511–517.
Goel, A., et al., 2018. Impaired perceptual learning in a mouse model of fragile X syndrome is mediated by parvalbumin neuron dysfunction and is reversible. Nat. Neurosci. 21, 1404–1411.
Grent-'t-Jong, T., et al., 2023. 40-Hz auditory steady-state responses in schizophrenia: toward a mechanistic biomarker for circuit dysfunctions and early detection and diagnosis. Biol. Psychiatry 94, 550–560.
Guyon, N., et al., 2021. Network asynchrony underlying increased broadband gamma power. J. Neurosci. 41, 2944–2963.
Hagerman, R.J., et al., 2009. Advances in the treatment of fragile X syndrome. Pediatrics 123, 378–390.
Hwang, E., et al., 2019. Optogenetic stimulation of basal forebrain parvalbumin neurons modulates the cortical topography of auditory steady-state responses. Brain Struct. Funct. 224, 1505–1518.
Jonak, C.R., et al., 2018. Reusable multielectrode array technique for electroencephalography in awake freely moving mice. Front. Integr. Neurosci. 12, 53.
Jonak, C.R., et al., 2020. Multielectrode array analysis of EEG biomarkers in a mouse model of fragile X syndrome. Neurobiol. Dis. 138, 104794.
Jonak, C.R., et al., 2021. The PDE10A inhibitor TAK-063 reverses sound-evoked EEG abnormalities in a mouse model of fragile X syndrome. Neurotherapeutics 18, 1175–1187.
Jonak, C.R., et al., 2022. Baclofen-associated neurophysiologic target engagement across species in fragile X syndrome. J. Neurodev. Disord. 14, 52.
Kenny, A., et al., 2022. EEG as a translational biomarker and outcome measure in fragile X syndrome. Transl. Psychiatry 12, 34.
Kim, H., et al., 2013. Impaired critical period plasticity in primary auditory cortex of fragile X model mice. J. Neurosci. 33, 15686–15692.
Korotkova, T., et al., 2010. NMDA receptor ablation on parvalbumin-positive interneurons impairs hippocampal synchrony, spatial representations, and working memory. Neuron 68, 557–569.
Kozono, N., et al., 2020. Gamma power abnormalities in a Fmr1-targeted transgenic rat model of fragile X syndrome. Sci. Rep. 10, 18799.
Kwon, J.S., et al., 1999. Gamma frequency-range abnormalities to auditory stimulation in schizophrenia. Arch. Gen. Psychiatry 56, 1001–1005.
Lee, A.W., et al., 2018. Clinical development of targeted fragile X syndrome treatments: an industry perspective. Brain Sci. 8.
Levy, R.B., et al., 2019. Circuit asymmetries underlie functional lateralization in the mouse auditory cortex. Nat. Commun. 10, 2783.
Lindell, A.K., Hudry, K., 2013. Atypicalities in cortical structure, handedness, and functional lateralization for language in autism spectrum disorders. Neuropsychol. Rev. 23, 257–270.
Lovelace, J.W., et al., 2016. Matrix metalloproteinase-9 deletion rescues auditory evoked potential habituation deficit in a mouse model of fragile X syndrome. Neurobiol. Dis. 89, 126–135.
Lovelace, J.W., et al., 2018. Translation-relevant EEG phenotypes in a mouse model of fragile X syndrome. Neurobiol. Dis. 115, 39–48.
Lovelace, J.W., et al., 2020. Deletion of Fmr1 from forebrain excitatory neurons triggers abnormal cellular, EEG, and behavioral phenotypes in the auditory cortex of a mouse model of fragile X syndrome. Cereb. Cortex 30, 969–988.
Maris, E., Oostenveld, R., 2007. Nonparametric statistical testing of EEG- and MEG-data. J. Neurosci. Methods 164, 177–190.
Miller, L.J., et al., 1999. Electrodermal responses to sensory stimuli in individuals with fragile X syndrome: a preliminary report. Am. J. Med. Genet. 83, 268–279.
Musumeci, S.A., et al., 1999. Epilepsy and EEG findings in males with fragile X syndrome. Epilepsia 40, 1092–1099.
Nakao, K., et al., 2020. GSK3beta inhibition restores cortical gamma oscillation and cognitive behavior in a mouse model of NMDA receptor hypofunction relevant to schizophrenia. Neuropsychopharmacology 45, 2207–2218.
O'Donnell, B.F., et al., 2013. The auditory steady-state response (ASSR): a translational biomarker for schizophrenia. Suppl. Clin. Neurophysiol. 62, 101–112.
Ono, Y., et al., 2020. Auditory steady-state response at 20 Hz and 40 Hz in young typically developing children and children with autism spectrum disorder. Psychiatry Clin. Neurosci. 74, 354–361.
Oswald, A.M., Reyes, A.D., 2011. Development of inhibitory timescales in auditory cortex. Cereb. Cortex 21, 1351–1361.
Oviedo, H.V., 2017. Connectivity motifs of inhibitory neurons in the mouse auditory cortex. Sci. Rep. 7, 16987.
Pastor, M.A., et al., 2002. Activation of human cerebral and cerebellar cortex by auditory stimulation at 40 Hz. J. Neurosci. 22, 10501–10506.
Pérez-Alcázar, M., et al., 2008. Chirp-evoked potentials in the awake and anesthetized rat. A procedure to assess changes in cortical oscillatory activity. Exp. Neurol. 210, 144–153.
Petersen, M.R., et al., 1978. Neural lateralization of species-specific vocalizations by Japanese macaques (Macaca fuscata). Science 202, 324–327.
Picton, T.W., et al., 2003. Human auditory steady-state responses. Int. J. Audiol. 42, 177–219.
Pressler, R., Auvin, S., 2013. Comparison of brain maturation among species: an example in translational research suggesting the possible use of bumetanide in newborn. Front. Neurol. 4, 36.
Purcell, D.W., et al., 2004. Human temporal auditory acuity as assessed by envelope following responses. J. Acoust. Soc. Am. 116, 3581–3593.
Ray, S., Maunsell, J.H., 2011. Different origins of gamma rhythm and high-gamma activity in macaque visual cortex. PLoS Biol. 9, e1000610.
Razak, K.A., et al., 2020. Developmental studies in fragile X syndrome. J. Neurodev. Disord. 12, 13.
Razak, K.A., et al., 2021. Neural correlates of auditory hypersensitivity in fragile X syndrome. Front. Psychol. 12, 720752.
Roberts, J.E., et al., 2001. Development and behavior of male toddlers with fragile X syndrome. J. Early Interv. 24, 207–223.
Rotschafer, S., Razak, K., 2013. Altered auditory processing in a mouse model of fragile X syndrome. Brain Res. 1506, 12–24.
Rotschafer, S.E., Razak, K.A., 2014. Auditory processing in fragile X syndrome. Front. Cell. Neurosci. 8, 19.
Rybalko, N., et al., 2010. Inactivation of the left auditory cortex impairs temporal discrimination in the rat. Behav. Brain Res. 209, 123–130.
Sabaratnam, M., et al., 2001. Epilepsy and EEG findings in 18 males with fragile X syndrome. Seizure 10, 60–63.
Schneider, A., et al., 2013. Electrocortical changes associated with minocycline treatment in fragile X syndrome. J. Psychopharmacol. 27, 956–963.

Semple, B.D., et al., 2013. Brain development in rodents and humans: identifying benchmarks of maturation and vulnerability to injury across species. Prog. Neurobiol. 106-107, 1–16.
Seymour, R.A., et al., 2020. Reduced auditory steady state responses in autism spectrum disorder. Mol. Autism. 11, 56.
Shannon, R.V., et al., 1995. Speech recognition with primarily temporal cues. Science 270, 303–304.
Sinclair, D., et al., 2017a. GABA-B agonist baclofen normalizes auditory-evoked neural oscillations and behavioral deficits in the Fmr1 knockout mouse model of fragile X syndrome. Eneuro 4. ENEURO.0380-16.2017.
Sinclair, D., et al., 2017b. Sensory processing in autism spectrum disorders and fragile X syndrome-from the clinic to animal models. Neurosci. Biobehav. Rev. 76, 235–253.
Sivarao, D.V., 2015. The 40-Hz auditory steady-state response: a selective biomarker for cortical NMDA function. Ann. N. Y. Acad. Sci. 1344, 27–36.
Spongr, V.P., et al., 1997. Quantitative measures of hair cell loss in CBA and C57BL/6 mice throughout their life spans. J. Acoust. Soc. Am. 101, 3546–3553.
Stroganova, T.A., et al., 2007. Abnormal EEG lateralization in boys with autism. Clin. Neurophysiol. 118, 1842–1854.
Swanson, M.R., et al., 2018. Development of white matter circuitry in infants with fragile X syndrome. JAMA Psychiat. 75, 505–513.
Tallal, P., et al., 1993. Neurobiological basis of speech: a case for the preeminence of temporal processing. Ann. N. Y. Acad. Sci. 682, 27–47.
Tallon-Baudry, C., et al., 1996. Stimulus specificity of phase-locked and non-phase-locked 40 Hz visual responses in human. J. Neurosci. 16, 4240–4249.
Uhlhaas, P.J., Singer, W., 2010. Abnormal neural oscillations and synchrony in schizophrenia. Nat. Rev. Neurosci. 11, 100–113.
Van der Molen, M.J., Van der Molen, M.W., 2013. Reduced alpha and exaggerated theta power during the resting-state EEG in fragile X syndrome. Biol. Psychol. 92, 216–219.
Van der Molen, M.J.W., et al., 2010. Profiling fragile X syndrome in males: strengths and weaknesses in cognitive abilities. Res. Dev. Disabil. 31, 426–439.
Vohs, J.L., et al., 2010. GABAergic modulation of the 40 Hz auditory steady-state response in a rat model of schizophrenia. Int. J. Neuropsychopharmacol. 13, 487–497.
Wang, X.J., Buzsaki, G., 1996. Gamma oscillation by synaptic inhibition in a hippocampal interneuronal network model. J. Neurosci. 16, 6402–6413.
Wang, J., et al., 2017. A resting EEG study of neocortical hyperexcitability and altered functional connectivity in fragile X syndrome. J. Neurodev. Disord. 9, 11.
Washington, S.D., Kanwal, J.S., 2012. Sex-dependent hemispheric asymmetries for processing frequency-modulated sounds in the primary auditory cortex of the mustached bat. J. Neurophysiol. 108, 1548–1566.
Wen, T.H., et al., 2018. Genetic reduction of matrix metalloproteinase-9 promotes formation of perineuronal nets around parvalbumin-expressing interneurons and normalizes auditory cortex responses in developing Fmr1 knock-out mice. Cereb. Cortex 28, 3951–3964.
Wen, T.H., et al., 2019. Developmental changes in EEG phenotypes in a mouse model of fragile X syndrome. Neuroscience 398, 126–143.
Wetzel, W., et al., 2008. Global versus local processing of frequency-modulated tones in gerbils: an animal model of lateralized auditory cortex functions. Proc. Natl. Acad. Sci. USA 105, 6753–6758.
Whittington, M.A., et al., 1995. Synchronized oscillations in interneuron networks driven by metabotropic glutamate receptor activation. Nature 373, 612–615.
Wisniewski, K.E., et al., 1991. The fra(X) syndrome: neurological, electrophysiological, and neuropathological abnormalities. Am. J. Med. Genet. 38, 476–480.
Yu, S., et al., 1991. Fragile X genotype characterized by an unstable region of DNA. Science 252, 1179–1181.
Zatorre, R.J., 2022. Hemispheric asymmetries for music and speech: Spectrotemporal modulations and top-down influences. Front. Neurosci. 16, 1075511.
Zhang, Z., et al., 2021. Experience-dependent weakening of callosal synaptic connections in the absence of postsynaptic FMRP. Elife 10, e71555.